Supporting Information

Single-molecule conductance studies on quasi- and metallaaromatic dibenzoylmethane coordination compounds and their aromatic analogs

André Mang,[a] Nils Rotthowe,[a] Katawoura Beltako,[b,c] Michael Linseis,[a] Fabian Pauly*[c] and Rainer F. Winter*[a]

[a]Chemistry Department, University of Konstanz, 78457 Konstanz, Germany. E-mail: rainer.winter@uni-konstanz.de

[b]Physics Department, University of Lomé, 1515 Lomé, Togo

[c]Institute of Physics, University of Augsburg, 86159 Augsburg, Germany. E-mail: fabian.pauly@uni-a.de

Materials and methods

Synthetic procedures

If not stated otherwise, all syntheses were carried out under inert conditions by applying standard SCHLENK techniques. The employed starting materials were purchased from commercial suppliers and used without further purification. Solvents were dried over appropriate drying agents, distilled and saturated with nitrogen prior to use.

NMR spectroscopy

^{1}H-, ^{13}C{^{1}H}-, ^{19}F{^{1}H}- and ^{31}P{^{1}H}-NMR spectra were either recorded on a BRUKER AVANCE III 400 MHz, a BRUKER AVANCE III HD 400 MHz, a BRUKER AVANCE III 600 MHz, a BRUKER AVANCE NEO 800 MHz or a JEOL 500 MHz spectrometer applying broadband decoupling at room temperature. Data processing was performed using the MNOVA software (MESTRELAB RESEARCH). Chemical shifts are reported in ppm and were referenced to the peak of the residual protonated solvent (^{1}H) or the solvent signal (^{13}C{^{1}H}) of the employed deuterated solvent, respectively. Spectral shifts in ^{19}F{^{1}H}- and ^{31}P{^{1}H}-NMR experiments were referenced by absolute techniques. All coupling constants are reported in Hertz (Hz). Signal assignments denoted with *H*-X/*H*-X' or *C*-X/*C*-X' correspond to resonances of both phenylene units within the dibenzoylmethane (DBM) scaffold or, in the case of **1SMe-RuP^{i}Pr$_3$**, resonances of two isomers within the sample.

X-ray diffraction analysis

Single crystals of **SMe-H**, **SMe-RhCOD**, and **SMe-RuP^{i}Pr$_3$** were grown by layer diffusion of *n*-pentane into dichloromethane solutions of the respective compound. Crystals of **SMe-BPh$^{F}_2$** were obtained by slow evaporation of a *n*-heptane solution of the compound. X-ray diffraction analysis was conducted on a STOE IPDS II diffractometer equipped with a graphite-monochromated Mo-K_α (λ = 0.71073 Å) or Cu-K_α (λ = 1.54186 Å) radiation source and an image plate detection system at T = 100 K. Data processing was carried out with the X-AREA software (STOE). Structure solution was accomplished by employing

OLEX2[1] in combination with the SHELXT[2] program. Further refinement was done using the SHELXL package.[3] Hydrogen atoms were introduced at their calculated positions. The evaluation of the obtained CIF files was carried out with MERCURY[4, 5] and Oak Ridge thermal ellipsoid plots (ORTEPs) were generated with PLATON.[6]

Scanning tunneling microscope break-junction (STM-BJ) measurements

Single-molecule conductance experiments were performed using a home-built STM-BJ setup according to the model of the VENKATARAMAN group at Columbia University, New York.[7, 8] The working principle of the setup corresponds to the fundamental routine for molecular junction formation in conventional STM measurements, as established by XU and TAO.[9] While monitoring the current at a constant bias voltage of 100 mV, a chemically etched gold tip is brought into physical contact with a gold platelet (substrate) until a predetermined conductance threshold is exceeded. The resulting many atom-thick electrode contact is then thinned out by withdrawing the substrate at a pull rate of 20 nm/s. On substrate withdrawal, individual Au-Au bonds successively break at the narrowest part of the atomic contact, which reduces the overall contact diameter. Accordingly, a stepwise conductance decrease with plateaus near integer values of G_0 ($\triangleq 2e^2/h \triangleq 77.48\ \mu S$)[10] on increasing substrate displacement is observed. The successful formation of a break junction is indicated by a steep exponential decay of the monitored current immediately after rupture of the last single-atom contact with a conductance of around $1G_0$. This break-junction formation routine is repeated several thousand times with a dilute solution of the analyte (0.5-1 mM) in 1,2,4-trichlorobenzene applied to the substrate under ambient conditions. During the experiments, the created nanogaps are statistically bridged by analyte molecules, leading to corresponding molecular conductance profiles. Due to the dependence of the observed conductance on atomic details of the relevant junction configuration, a significant conductance value cannot be extracted from a single experiment. Therefore, a minimum of 4500 individual molecular conductance *versus* displacement traces for each of the investigated compounds was recorded and logarithmically binned into histograms to ensure the statistical relevance of the acquired data. The same experiments were also conducted on the pure solvent in order to evaluate the solvent background. To ensure the comparability of the respective single-molecule charge transport characteristics of the target compounds, the obtained conductance distributions were subsequently normalized.[7, 8] The operation of the setup and general data processing were carried out with the IGOR PRO 8 software (WAVEMETRICS, INC.), employing customized operation and analysis implementations provided by the VENKATARAMAN group.[7, 8] Data analysis was accomplished using an unmodified version of the code.

Additional STM-BJ measurements

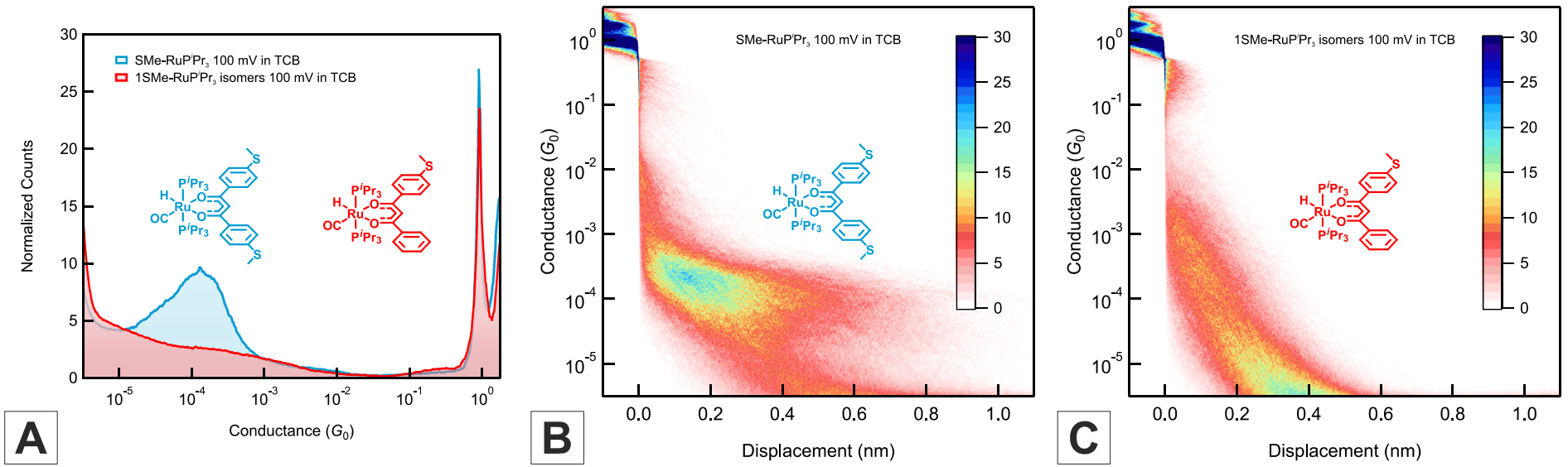

Figure S1 | (**A**) Logarithmically binned 1D conductance histogram of **SMe-RuP^{i}Pr$_3$** and an isomeric mixture of **1SMe-RuP^{i}Pr$_3$** in a 1,2,4-trichlorobenzene (TCB) solution at 100 mV bias voltage. (**B**) and (**C**) 2D conductance-displacement histograms of **SMe-RuP^{i}Pr$_3$** and isomeric **1SMe-RuP^{i}Pr$_3$**. All histograms were constructed from 5000 traces and binned without data selection.

Computational details

Electronic structure and contact geometries were determined within the framework of density functional theory (DFT). DFT calculations were performed, as implemented in the TURBOMOLE quantum chemistry software package.[11] We used the exchange-correlation functional of PERDEW, BURKE and ERNZERHOF (PBE)[12, 13] and the default basis set of split-valence-plus-polarization quality def-SV(P).[14] Total energies were converged to a precision of better than 10^{-6} a.u., and geometries were optimized until the maximum norm of the Cartesian gradient was less than 10^{-5} a.u. The extended central cluster[15] of all junction geometries studied consists of two gold pyramids, oriented in the crystallographic direction (111). On one end of the model junctions the corresponding test molecule is either attached *via* a sulfur atom to the tip atom of a Au_{20} pyramid, which we denote as 'top' binding, or to a blunt Au_{19} pyramid, where the tip atom is removed. We term this kind of binding as 'hollow' binding, although we find that the SMe anchor group arranges in such a way as to attach to a single Au atom on the three-atom pyramidal trunk (see Figure S2). In each case the geometry of the extended central cluster was optimized by energy minimization, while keeping the two outermost layers fixed at ideal face-centered cubic lattice positions.

Electrical transport properties were determined within the phase coherent limit using the LANDAUER-BÜTTIKER formalism.[15-17] Employing linear response theory, we express the conductance as

$$G = G_0 \int_{-\infty}^{\infty} dE \left(-\frac{\partial f}{\partial E} \right) \tau(E).$$

We evaluated the energy-dependent transmission function $\tau(E)$ through nonequilibrium GREEN's function techniques, utilizing the DFT-based electronic structure of the static ground state geometries. At sufficiently low temperatures the electrical conductance is described by $G = G_0 \tau(E)$, and we used this simplified formula throughout this work to determine the conductance directly from the transmission.

In order to correct for known deficiencies of DFT, we compute electronic transmissions, besides using the pure DFT electronic structure, additionally from the DFT+Σ method.[18-21] This correction scheme provides more accurate energy gaps of the isolated molecule and accounts for the electronic screening of the connected macroscopic, metallic gold electrodes by image charges in the junction geometries. The computationally derived Fermi energy E_F of the gold electrodes is -5.0 eV.

A comparison of energy-dependent transmission curves from DFT and DFT+Σ is shown in Figure S2. In the charge transport studies we constructed electrode GREEN's functions in real space, assuming periodic boundary conditions perpendicular to the transport direction and a periodicity of 42×42 lattice sites.[15] For DFT+Σ, the image charge plane was located 1.4 Å in front of the first fixed Au atomic layer of the extended central cluster, when viewed from the molecule.[21]

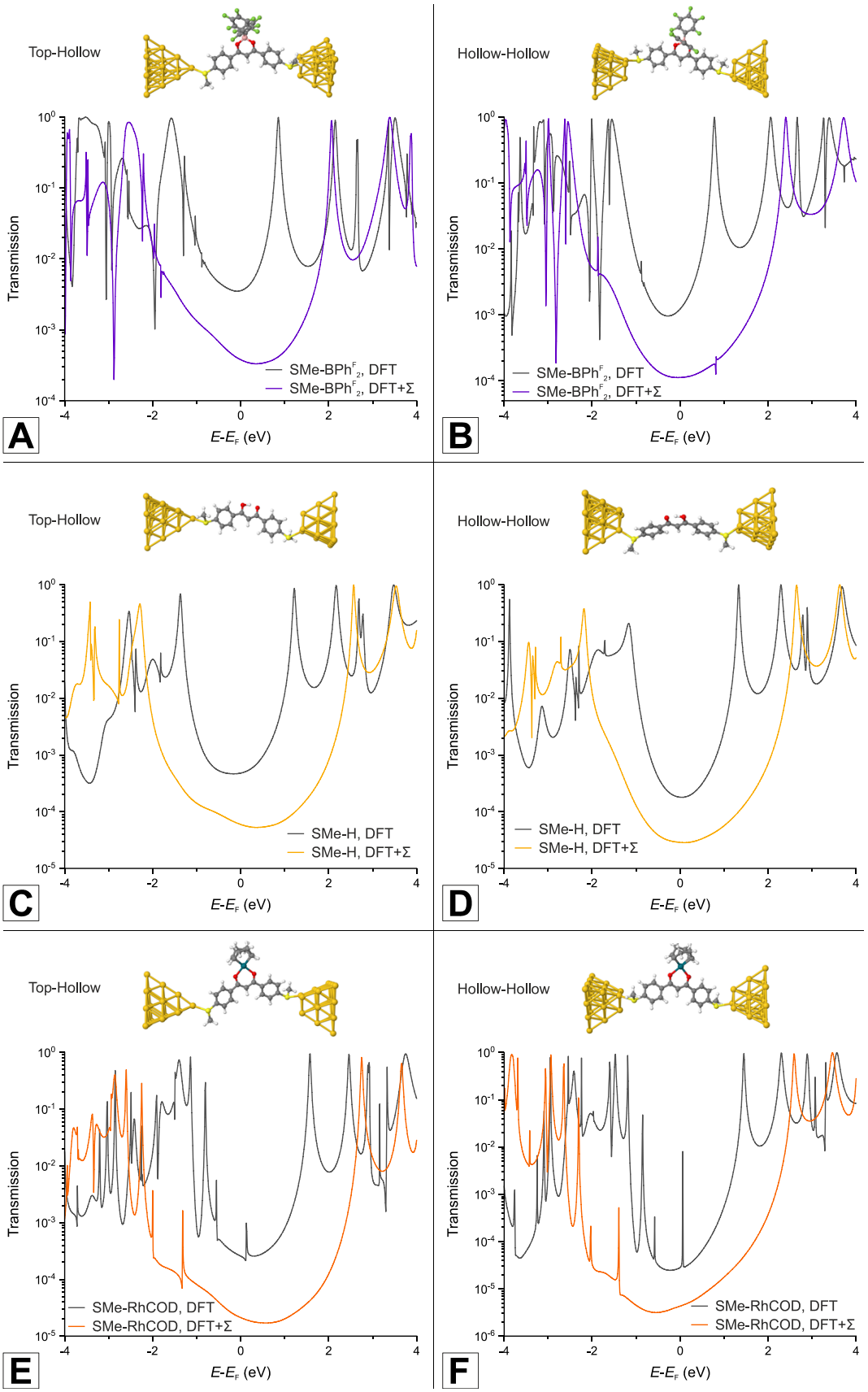

Figure S2 | Transmission of the three molecular junctions as a function of energy, obtained from DFT and DFT+Σ calculations, in (**A**, **C**, **E**) top-hollow and (**B**, **D**, **F**) hollow-hollow configurations. The corresponding extended central clusters of top-hollow (left column) and hollow-hollow (right column) configurations are shown above each transmission plot.

Conductances for top-hollow and hollow-hollow configurations

Similar to the top-top junctions, discussed in the main text, we studied top-hollow and hollow-hollow configurations by removing the tip gold atom on one or at both gold electrodes. As shown in Figure S2, the sulfur atom of the SMe anchor group was found to always connect to a single gold atom at the atomically sharp tip or the blunt three-atom trunk. Plots of the energy-dependent transmission are provided in Figure S2. The extracted conductance values are summarized in Table S1. The same ordering of conductances G(**SMe-BPh$^{F}_{2}$**) > G(**SMe-H**) > G(**SMe-RhCOD**) was found irrespective of the precise binding geometry for all three considered configurations, i.e. top-top, top-hollow and hollow-hollow.

Table S1 | Summary of conductance values calculated with the DFT+Σ method for the three types of molecular junctions in top-hollow and hollow-hollow configurations.

	Top-Hollow			Hollow-Hollow		
Compound	**SMe-BPh$^{F}_{2}$**	**SMe-H**	**SMe-RhCOD**	**SMe-BPh$^{F}_{2}$**	**SMe-H**	**SMe-RhCOD**
Conductance (G_0)	3.79×10^{-4}	5.96×10^{-5}	2.12×10^{-5}	1.13×10^{-4}	2.88×10^{-5}	4.32×10^{-6}

Orbitals analysis

Figure S3 shows molecular orbitals of the three isolated molecules. For the top-top geometry presented in Figure 3 of the manuscript, transport is clearly dominated by the highest occupied molecular orbital (HOMO) or the HOMO-1 state. This remains true for the top-hollow geometries shown in Figure S2, but less so for the hollow-hollow ones. For **SMe-BPh$^{F}_{2}$** and **SMe-H** the delocalized HOMO states are the main contributors to the transmission at E_F. Indeed, all frontier orbitals of **SMe-H** from HOMO-1 to LUMO+1 well extend over the entire molecule. For **SMe-BPh$^{F}_{2}$**, states that are localized mainly on the BPh$^{F}_{2}$ unit are found right below the HOMO, where they cause narrow FANO resonance-antiresonance features. Note also that the HOMO of **SMe-BPh$^{F}_{2}$** exhibits a node at the boron center, similar to the transmission eigenchannel shown in panel C of Figure 3. For **SMe-RhCOD**, the HOMO is confined to the RhCOD fragment within the DBM binding pocket. This localized state causes the narrow FANO resonance located 1.5 to 2 eV below E_F, and charge transport hence proceeds mainly through the delocalized HOMO-1, to which the entire π-(cross-)conjugated DBM backbone and the RhCOD entity contribute. The metal states of Rh participate in conduction and open an alternative transport pathway in **SMe-RhCOD**, which results from the mixing of the rhodium d_π-orbitals with the p_π-orbitals of the ketoenolate oxygen donor atoms. Interestingly, our orbital analysis indicates the occurrence of constructive quantum interference for all the three studied molecules, as it is visible from the parities of delocalized HOMO (or HOMO-1 for **SMe-RhCOD**) and LUMO frontier orbital wave functions on the terminal sulfur atoms.[22, 23]

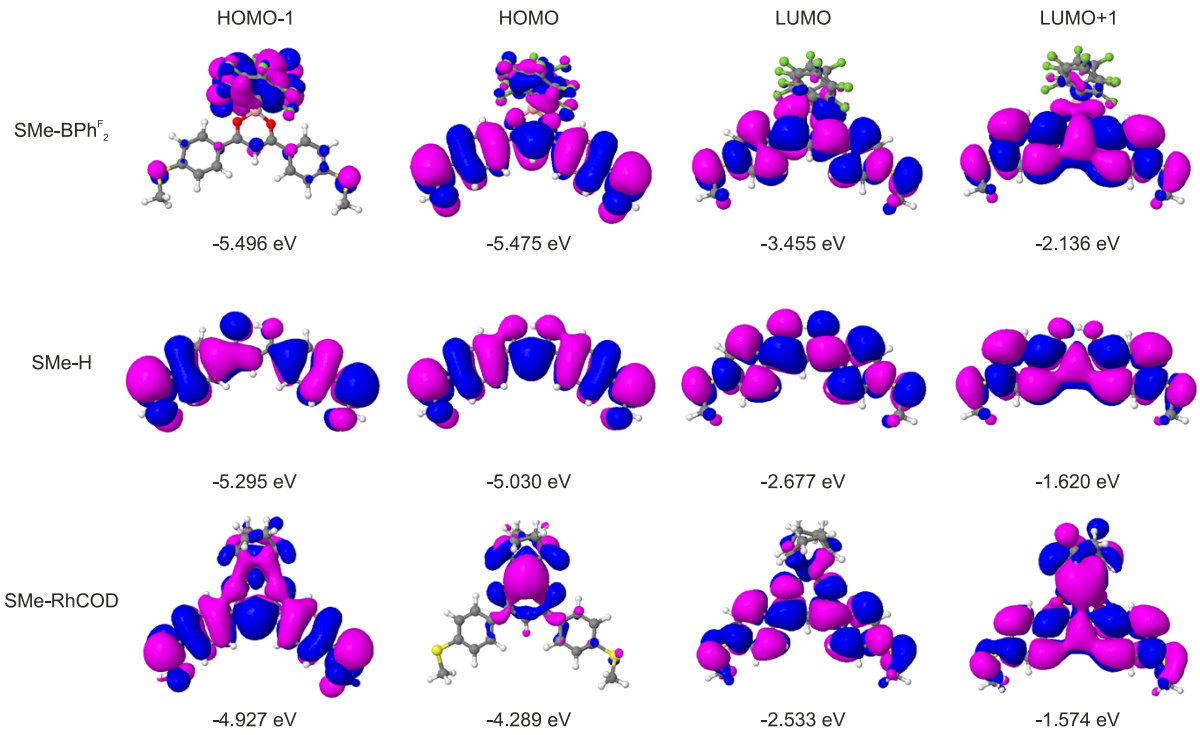

Figure S3 | Molecular frontier orbitals of the three isolated molecules **SMe-BPh$^{F}_{2}$**, **SMe-H**, and **SMe-RhCOD**.

Calculation of the nucleus-independent chemical shift (NICS)

In order to probe for potential aromaticity in **SMe-BPh$^{F}_{2}$** and **SMe-RhCOD** as representative model compounds, a dummy centroid (i.e. a dummy atom without nuclear charge, but with the basis functions of ^{3}He),[24] was placed inside the central ring of the respective optimized geometries. NICS values are per definition the negative of the nuclear magnetic resonance (NMR) shielding values, which were calculated within the Gauge-Including Atomic Orbital (GIAO) method, as implemented in the TURBOMOLE quantum chemistry package.[11] Here, we employed the exchange-correlation functional of PERDEW, BURKE and ERNZERHOF (PBE)[12, 13] in combination with the default basis set of split-valence-plus-polarization quality def-SV(P).[14] The obtained NICS(0) values are consistent with those calculated with other auxiliary basis sets such as def2-TZVP and def2-QZVP[14] as well as with the results of GAUSSIAN 16 calculations,[25] employing the same functional and basis set combinations (see Table S2).

Table S2 | Computed NICS(0) values for **SMe-RhCOD** and **SMe-BPh$^{F}_{2}$**, employing the GIAO method, as implemented in TURBOMOLE.

Compound	**NICS(0)**		
	PBE/def-SV(P)	PBE/def2-TZVP	PBE/def2-QZVP
SMe-RhCOD	-2.46 / -1.33[a)]	-1.78	-1.67
SMe-BPh$^{F}_{2}$	+2.07 / +2.19[a)]	+2.84	+2.85

a) Values were calculated with GAUSSIAN 16.

Synthesis and Characterization

3-Hydroxy-1,3-bis(4-(methylthio)phenyl)prop-2-en-1-one (SMe-H)

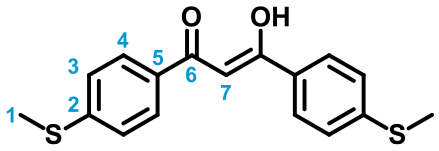

SMe-H

4-(Methylthio)acetophenone (1.27 g, 7.64 mmol, 1.0 eq) was added in small portions to a suspension of sodium hydride (60 wt% in mineral oil, 0.37 g, 9.17 mmol, 1.2 eq) in dry tetrahydrofuran (100 mL) at room temperature. The onset of the reaction was indicated by hydrogen evolution. Stirring was continued for 30 min after hydrogen gas evolution had ceased. Afterwards, ethyl 4-(methylthio)benzoate (1.50 g, 7.64 mmol, 1.0 eq) was added dropwise. The mixture was heated at reflux for 16 h. Evaporation of volatile components *in vacuo* gave an orange residue, which was extracted with ethyl acetate (50 mL) and washed with a saturated aqueous solution of ammonium chloride (50 mL). The layers were separated and the organic phase was dried over sodium sulfate, followed by the removal of the solvent under reduced pressure. Recrystallization of the crude product from ethanol afforded **SMe-H** in the form of golden-yellow crystals in 35% yield (0.86 g, 2.72 mmol).

^{1}H-NMR (500 MHz, $(CD_3)_2CO$): δ (ppm) = 8.06 (d, $^{3}J_{HH}$ = 8.4 Hz, 4H, *H*-4), 7.39 (d, $^{3}J_{HH}$ = 8.4 Hz, 4H, *H*-3), 7.18 (s, 1H, *H*-7), 2.57 (s, 6H, *H*-1).

^{13}C{^{1}H}-NMR (126 MHz, $(CD_3)_2CO$): δ (ppm) = 185.9 (s, *C*-6), 146.6 (s, *C*-2), 132.5 (s, *C*-5), 128.7 (s, *C*-4), 126.1 (s, *C*-3), 93.0 (s, *C*-7), 14.7 (s, *C*-1).

3-Hydroxy-1-(4-(methylthio)phenyl)-3-phenylprop-2-en-1-one (1SMe-H)

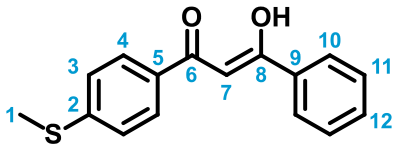

1SMe-H

4-(Methylthio)acetophenone (2.50 g, 15.04 mmol, 1.0 eq) was added in small portions to a suspension of sodium hydride (60 wt% in mineral oil, 0.72 g, 18.00 mmol, 1.2 eq) in dry tetrahydrofuran (100 mL) at room temperature. The onset of the reaction was indicated by hydrogen evolution. Stirring was continued for 30 min after hydrogen gas evolution had ceased. Afterwards, ethyl benzoate (2.16 mL, 2.26 g, 15.04 mmol, 1.0 eq) was added dropwise. The mixture was heated at reflux for 16 h. The evaporation of all volatile components *in vacuo* gave an orange residue, which was extracted with ethyl acetate (50 mL) and washed with a saturated aqueous solution of ammonium chloride (50 mL). The layers were separated, and the organic phase was dried over sodium sulfate, followed by the removal of the solvent under reduced pressure. Recrystallization of the crude product from methanol afforded **1SMe-H** as yellow crystals in 30% yield (1.22 g, 4.51 mmol).

^{1}H-NMR (400 MHz, $(CD_3)_2CO$): δ (ppm) = 17.31 (bs, 1H, O*H*), 8.17-8.06 (m, 4H, *H*-4+*H*-10), 7.61-7.48 (m, 3H, *H*-11+*H*-12), 7.40 (d, $^3J_{HH}$ = 8.6 Hz, 2H, *H*-3), 7.22 (s, 1H, *H*-7), 2.57 (s, 3H, *H*-1).

(1,3-Bis(4-methylthiophenyl)propane-1,3-diketonato)boron difluoride (SMe-BF$_2$)

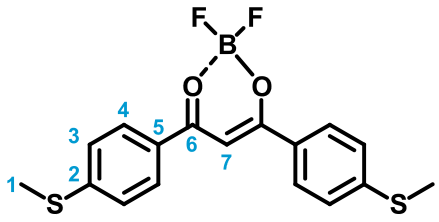

SMe-BF$_2$

Boron trifluoride diethyl etherate (30 µL, 33.6 mg, 237 µmol, 1.5 eq) was added to a solution of **SMe-H** (50 mg, 158 µmol, 1.0 eq) in dry dichloromethane (10 mL) and the mixture was stirred at room temperature for 16 h. The luminescent solution was evaporated to dryness, and the solid residue was extracted with a mixture of acetone and *n*-heptane (40 mL, 1:1 *v*/*v*). The solution was concentrated under reduced pressure, which caused the precipitation of a fine powder. The crude product was collected by filtration and washed with *n*-heptane (2 × 20 mL). Recrystallization from a mixture of acetone and *n*-heptane (1:1 *v*/*v*) gave **SMe-BF$_2$** in the form of ochre crystals in 72% yield (41.5 mg, 114 µmol).

^{1}H-NMR (600 MHz, $CDCl_3$): δ (ppm) = 8.03 (d, $^3J_{HH}$ = 8.5 Hz, 4H, *H*-4), 7.33 (d, $^3J_{HH}$ = 8.5 Hz, 4H, *H*-3), 7.07 (s, 1H, *H*-7), 2.57 (s, 6H, *H*-1).

^{13}C{^{1}H}-NMR (151 MHz, $CDCl_3$): δ (ppm) = 181.4 (s, *C*-6), 149.7 (s, *C*-2), 129.2 (s, *C*-4), 128.0 (s, *C*-5), 125.3 (s, *C*-3), 92.4 (s, *C*-7), 14.8 (s, *C*-1).

^{19}F{^{1}H}-NMR (376 MHz, $CDCl_3$): δ (ppm) = -140.51 (s, $^{10}BF_2$), -140.57 (s, $^{11}BF_2$).

Bis(pentafluorophenyl)boron-1,3-bis(4-(methylthio)phenyl)propane-1,3-diketonate (SMe-BPh$^F_2$)

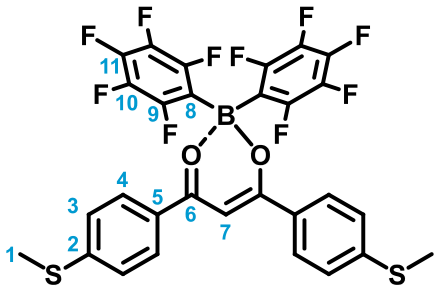

SMe-BPh$^F_2$

Tris(pentafluorophenyl)borane (150 mg, 293 µmol, 1 eq) was added to a solution of **SMe-H** (92.7 mg, 293 µmol, 1 eq) in dry toluene (70 mL), and the reaction mixture was stirred at room temperature for 16 h. The resulting luminescent solution was evaporated to dryness. The solid residue was repeatedly crystallized from *n*-heptane, affording **SMe-BPh$^F_2$** as orange crystals in 41% yield (80 mg, 121 µmol).

^{1}H-NMR (600 MHz, $CDCl_3$): δ (ppm) = 8.06 (d, $^{3}J_{HH}$ = 8.6 Hz, 4H, *H*-4), 7.35 (d, $^{3}J_{HH}$ = 8.6 Hz, 4H, *H*-3), 7.01 (s, 1H, *H*-7), 2.57 (s, 6H, *H*-1).

^{13}C{^{1}H}-NMR (151 MHz, $CDCl_3$): δ (ppm) = 181.2 (s, *C*-6), 150.1 (s, *C*-2), 148.3 (dm, $^{1}J_{CF}$ = 243.4 Hz, *C*-9/*C*-10), 140.4 (dm, $^{1}J_{CF}$ = 250.5 Hz, *C*-11), 137.2 (dm, $^{1}J_{CF}$ = 249.7 Hz, *C*-9/*C*-10), 129.4 (s, *C*-4), 128.0 (s, *C*-5), 125.3 (s, *C*-3), 117.0-115.6 (m, *C*-8), 92.8 (s, *C*-7), 14.8 (s, *C*-1).

^{19}F{^{1}H}-NMR (753 MHz, $CDCl_3$): δ (ppm) = -135.82 to -135.97 (m, *F*-9/*F*-10), -156.95 (t, $^{3}J_{FF}$ = 20.2 Hz, *F*-11), -163.73 to -163.87 (m, *F*-9/*F*-10).

(1,3-Bis(4-methylthiophenyl)propane-1,3-diketonato)(1,5-cyclooctadiene)rhodium(I) (SMe-RhCOD)

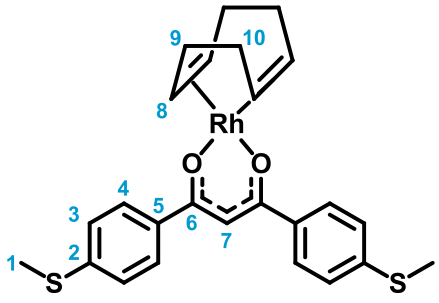

SMe-RhCOD

An aqueous solution of potassium hydroxide (68 mg, 1218 µmol, 2.5 eq) in deionized water (20 mL) was added to a solution of **SMe-H** (154 mg, 487 µmol, 1.0 eq) in diethyl ether (30 mL) under ambient conditions. A solution of the chloro(1,5-cyclooctadiene)rhodium(I) dimer (120 mg, 243 µmol, 0.5 eq) in diethyl ether (20 mL) was added to the biphasic mixture and the reaction mixture was stirred at room temperature for 16 h. The layers were separated, the organic phase was washed with deionized water (3 × 10 mL), dried over sodium sulfate, and the volatiles were removed under reduced pressure. Recrystallization of the crude product from *n*-heptane furnished **SMe-RhCOD** in form of yellow acicular crystals in 83% yield (213 mg, 405 µmol).

^{1}H-NMR (600 MHz, $CDCl_3$): δ (ppm) = 7.75 (d, $^{3}J_{HH}$ = 8.4 Hz, 4H, *H*-4), 7.21 (d, $^{3}J_{HH}$ = 8.4 Hz, 4H, *H*-3), 6.59 (s, 1H, *H*-7), 4.28-4.22 (m, 4H, *H*-8), 2.56-2.51 (m, 4H, *H*-9), 2.50 (s, 6H, *H*-1), 1.95-1.86 (m, 4H, *H*-10).

^{13}C{^{1}H}-NMR (151 MHz, $CDCl_3$): δ (ppm) = 180.5 (s, *C*-6), 142.6 (s, *C*-2), 136.1 (s, *C*-5), 127.8 (s, *C*-4), 125.4 (s, *C*-3), 93.2 (s, *C*-7), 77.1 (d, $^{1}J_{CRh}$ = 14.1 Hz, *C*-8), 30.5 (s, *C*-9, *C*-10), 15.3 (s, *C*-1).

Carbonylhydrido(1,3-bis(4-methylthiophenyl)propane-1,3-diketonato)bis(triisopropylphosphane)ruthenium(II) (SMe-RuP^{i}Pr$_3$)

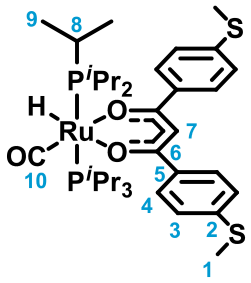

SMe-RuP^{i}Pr$_3$

Carbonylchlorohydridobis(triisopropylphosphane)ruthenium(II) (HRu(CO)Cl(P^{i}Pr$_3$)$_2$, 76.8 mg, 158 µmol, 1 eq) was added to a suspension of **SMe-H** (50.0 mg, 158 µmol, 1 eq) and potassium carbonate (109.2 mg, 790 µmol, 5 eq) in a solvent mixture of dry dichloromethane (5 mL) and methanol (3 mL). The reaction mixture was stirred at room temperature for 16 h, and the liquid layer was decanted after centrifugation. The red precipitate was dissolved in dichloromethane (5 mL) and insoluble contaminants were filtered off. The filtrate was evaporated to dryness and the crude product was washed with methanol (3 × 5 mL). Drying *in vacuo* furnished **SMe-RuP^{i}Pr$_3$** as a red powder in 74% yield (89.6 mg, 117 µmol).

^{1}H-NMR (600 MHz, CD_2Cl_2): δ (ppm) = 7.85 (d, $^3J_{HH}$ = 8.4 Hz, 2H, *H*-4/*H*-4'), 7.78 (d, $^3J_{HH}$ = 8.4 Hz, 2H *H*-4/*H*-4'), 7.24 (d, $^3J_{HH}$ = 8.4 Hz, 2H, *H*-3/*H*-3'), 7.20 (d, $^3J_{HH}$ = 8.4 Hz, 2H, *H*-3/*H*-3'), 6.56 (s, 1H, *H*-7), 2.52 (s, 3H, *H*-1/*H*-1'), 2.50 (s, 3H, *H*-1/*H*-1'), 2.26-2.17 (m, 6H, *H*-8), 1.32 (vq, 18H, *J* = 6.6 Hz, *H*-9/*H*-9'), 1.19 (vq, *J* = 6.6 Hz, 18H, *H*-9/*H*-9'), -15.07 (t, $^2J_{HP}$ = 19.6 Hz, 1H, *H*-Ru).

^{13}C{^{1}H}-NMR (151 MHz, CD_2Cl_2): δ (ppm) = 208.7 (t, $^2J_{CP}$ = 14.7 Hz, *C*-10), 182.6 (s, *C*-6/*C*-6'), 179.5 (s, *C*-6/*C*-6'), 141.8 (s, *C*-2/*C*-2'), 141.7 (s, *C*-2/*C*-2'), 138.5 (s, *C*-5/*C*-5'), 138.0 (s, *C*-5/*C*-5'), 127.8 (s, *C*-4/*C*-4'), 127.7 (s, *C*-4/*C*-4'), 125.6 (s, *C*-3/*C*-3'), 125.5 (s, *C*-3/*C*-3'), 92.8 (s, *C*-7), 25.2 (t, $^1J_{CP}$ = 9.3 Hz, *C*-8), 20.2 (s, *C*-9/*C*-9'), 19.6 (s, *C*-9/*C*-9'), 15.5 (s, *C*-1/*C*-1'), 15.5 (s, *C*-1/*C*-1').

Signal assignments denoted with ' correspond to H/C atoms at the opposite phenylene unit of the dibenzoylmethane moiety or magnetically different tri^{iso}propylphosphine ligands.

^{31}P{^{1}H}-NMR (243 MHz, CD_2Cl_2): δ (ppm) = 55.70-54.60 (m, *P*^{i}Pr$_3$).

Carbonylhydrido(1-(4-methylthiophenyl)-3-phenylpropane-1,3-diketonato)bis(triisopropylphosphane)ruthenium(II) (SMe-RuP^{i}Pr$_3$)

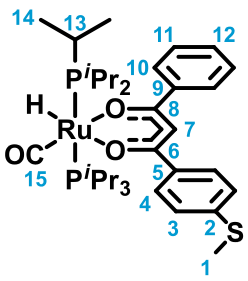

1SMe-RuP^{i}Pr$_3$

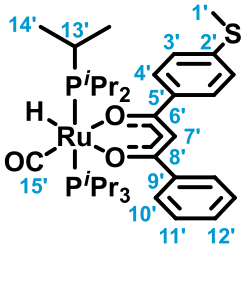

1SMe*-RuP^{i}Pr$_3$

Carbonylchlorohydridobis(triisopropylphosphane)ruthenium(II) (HRu(CO)Cl(P^{i}Pr$_3$)$_2$, 180.0 mg, 0.37 mmol, 1 eq) was added to a suspension of **1SMe-H** (100.0 mg, 0.37 µmol, 1 eq) and potassium carbonate (256.0 mg, 1.85 mmol, 5 eq) in a solvent mixture of dry dichloromethane (10 mL) and methanol (5 mL). The reaction mixture was stirred at room temperature for 16 h. The liquid layer was decanted, and the solvent was removed under reduced pressure. The orange residue was dissolved in dichloromethane (5 mL), and insoluble contaminants were filtered off. The filtrate was evaporated to dryness, and the crude product was washed with methanol (5 × 5 mL). Drying *in vacuo* furnished **1SMe-RuP^{i}Pr$_3$** as an orange powder in 67% yield (184.0 mg, 0.25 mmol).

The title compound was obtained in an isomeric mixture with **1SMe*-RuP^{i}Pr$_3$**.

^{1}H-NMR (400 MHz, CD_2Cl_2): δ (ppm) = 7.93-7.76 (m, 4H, *H*-4/*H*-4'+*H*-10/*H*-10'), 7.46-7.31 (m, 3H, *H*-11/*H*-11'+*H*-12/*H*-12'), 7.28-7.16 (m, 2H, *H*-3/*H*-3'), 6.59 (bs, 1H, *H*-7/*H*-7'), 2.53-2.49 (m, 3H, *H*-1/*H*-1'), 2.31-2.15 (m, 6H, *H*-13/*H*-13'), 1.38-1.27 (m, 18H, *H*-14/*H*-14'), 1.25-1.14 (m, 18H, *H*-14/*H*-14'), -15.00 to -15.15 (m, 1H, *H*-Ru/*H*-Ru').

^{13}C{^{1}H}-NMR (101 MHz, CD_2Cl_2): δ (ppm) = 208.9-208.4 (m, *C*-15/ *C*-15'), 183.6 (s, *C*-8/*C*-8'), 182.9 (s, *C*-8/*C*-8'), 180.4 (s, *C*-6/*C*-6'), 179.7 (s, *C*-6/*C*-6'), 142.2 (s, *C*-9/*C*-9'), 141.9-141.8 (m, *C*-2/*C*-2'), 141.7 (s, *C*-9/*C*-9'), 138.5 (s, *C*-5/*C*-5'), 138.0 (s, *C*-5/*C*-5'), 130.4-130.3 (m, *C*-12/*C*-12'), 128.7-128.4 (m, *C*-11/*C*-11'), 127.9-127.6 (m, *C*-4/*C*-4'), 127.4-127.1 (m, *C*-10/*C*-10'), 125.8-125.4 (m, *C*-3/*C*-3'), 93.4 (bs, *C*-7/*C*-7'), 25.4-25.0 (m, *C*-13/*C*-13'), 20.2 (bs, *C*-14/*C*-14'), 19.7-19.5 (m, *C*-14/*C*-14'), 15.6-15.4 (m, *C*-1/*C*-1').

^{31}P{^{1}H}-NMR (162 MHz, CD_2Cl_2): δ (ppm) = 54.64 (s, *P*^{i}Pr$_3$/*P*^{i}Pr$_3$'), 54.61 (s, *P*^{i}Pr$_3$/*P*^{i}Pr$_3$').

Signal assignments denoted with ' correspond to H/C atoms at the opposite phenylene unit of the dibenzoylmethane moiety, magnetically different tri^{iso}propylphosphine ligands and different isomers.

4,6-Bis(4-(methylthio)phenyl)benzene (SMe-TerPh)

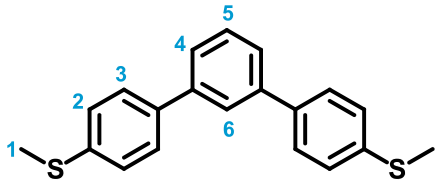

SMe-TerPh

A suspension of 1,3-diiodobenzene (247 mg, 0.75 mmol, 1.0 eq), 4-methylthiophenylboronic acid (504 mg, 3.00 mmol, 4 eq) and K_3PO_4 (796 mg, 3.75 mmol, 5 eq) in 1,4-dioxane (60 mL) was thoroughly degassed and subsequently saturated with nitrogen. Catalytic amounts of [1,1'-bis(diphenylphosphino)ferrocene]palladium(II) dichloride (55 mg, 75 µmol, 0.1 eq) were added, and the mixture was stirred at 70 °C for 16 h. The volatiles were removed under reduced pressure and the black residue was extracted with toluene (50 mL). Insoluble contaminants were removed *via* filtration over Celite, and the filtrate was consecutively washed with an aqueous solution of sodium hydroxide (1 M, 2 × 50 mL) and deionized water (2 × 50 mL). The organic layer was dried over sodium sulfate and evaporated to dryness. Successive recrystallization of the crude product from *n*-heptane and methanol gave **SMe-TerPh** in the form of a solid with a silverish shine in 16% yield (40 mg, 124 µmol).

^{1}H-NMR (400 MHz, $CDCl_3$): *δ* (ppm) = 7.75 (t, $^4J_{HH}$ = 1.5 Hz, 1H, *H*-6), 7.57 (d, $^3J_{HH}$ = 8.5 Hz, 4H, *H*-3), 7.55-7.46 (m, 3H, *H*-4, *H*-5), 7.35 (d, $^3J_{HH}$ = 8.5 Hz, 4H, *H*-2), 2.54 (s, 6H, *H*-1).

4,6-Bis(4-(methylthio)phenyl)pyrimidine (SMe-TerY)

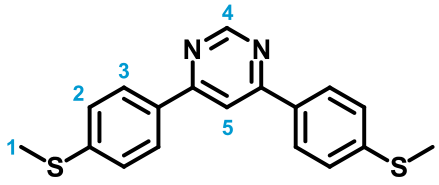

SMe-TerY

A suspension of 4,6-dichloropyrimidine (100 mg, 0.67 mmol, 1.0 eq), 4-methylthiophenylboronic acid (282 mg, 1.68 mmol, 2.5 eq) and K_3PO_4 (711 mg, 3.35 mmol, 5.0 eq) in 1,4-dioxane (20 mL) was thoroughly degassed and subsequently saturated with nitrogen. Catalytic amounts of [1,1'-bis(diphenylphosphino)ferrocene]palladium(II) dichloride (49 mg, 67 µmol, 0.1 eq) were added, and the reaction mixture was stirred at 80 °C for 24 h. The volatiles were removed under reduced pressure, and the black residue was extracted with dichloromethane (50 mL). Insoluble contaminants were removed *via* filtration over Celite, and the filtrate was washed with deionized water (2 × 40 mL). The organic layer was dried over magnesium sulfate, and the solvent was evaporated *in vacuo*. Purification of the crude product by column chromatography over silica gel (ethyl acetate/dichloromethane, 1:4 *v*/*v*) and subsequent recrystallization from *n*-heptane furnished **SMe-TerY** as pale yellow needles in 34% yield (74 mg, 228 µmol).

^{1}H-NMR (400 MHz, $CDCl_3$): *δ* (ppm) = 9.25 (s, 1H, *H*-4), 8.08 (d, $^3J_{HH}$ = 8.2 Hz, 4H, *H*-3), 8.03 (s, 1H, *H*-5), 7.38 (d, $^3J_{HH}$ = 8.2 Hz, 4H, *H*-2), 2.56 (s, 6H, *H*-1).

NMR spectra

SMe-H

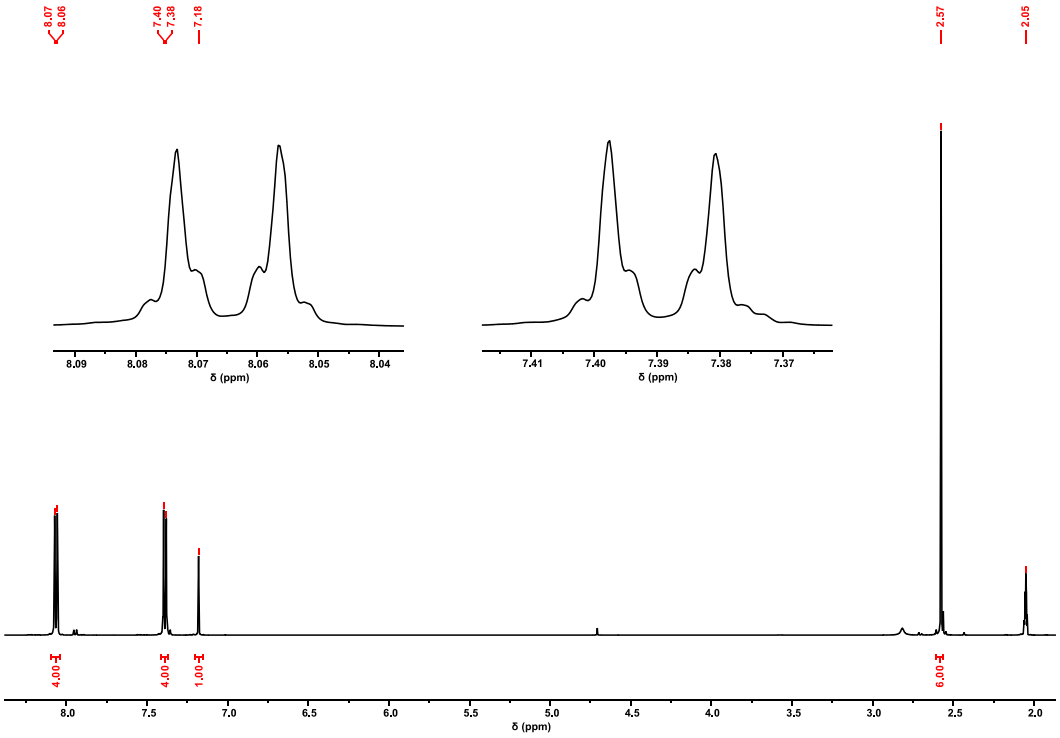

Figure S4 | **^{1}H-NMR** (500 MHz, $(CD_3)_2CO$), rt) spectrum of **SMe-H**.

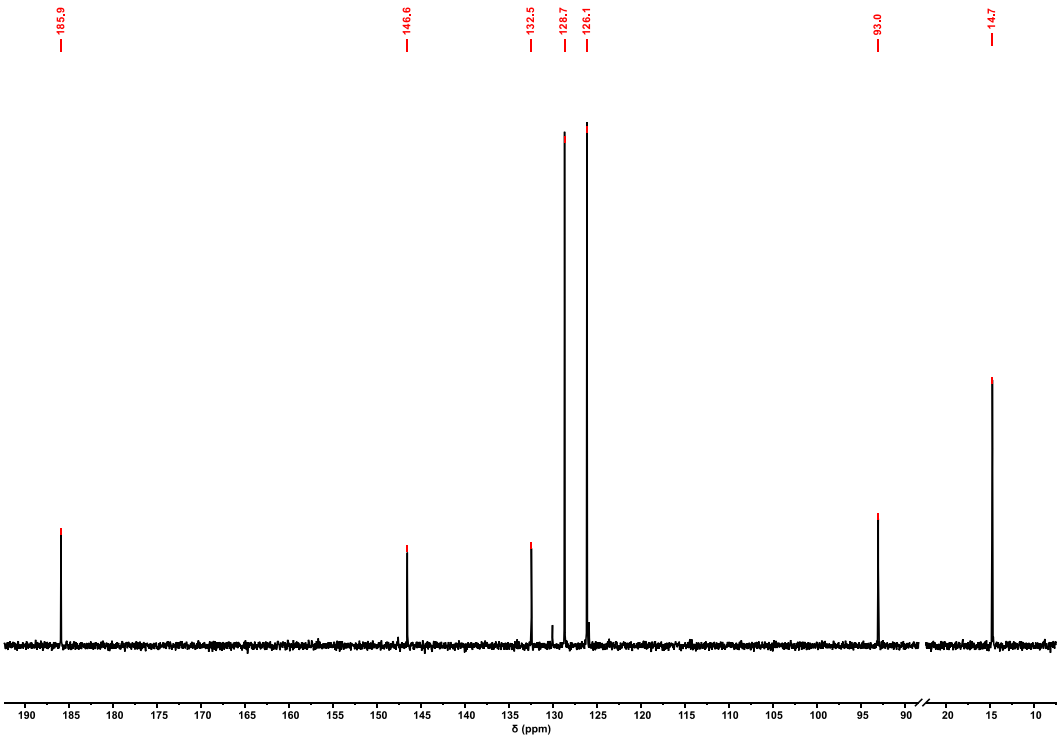

Figure S5 | **^{13}C{^{1}H}-NMR** (126 MHz, $(CD_3)_2CO$, rt) spectrum of **SMe-H**.

SMe-BF_2

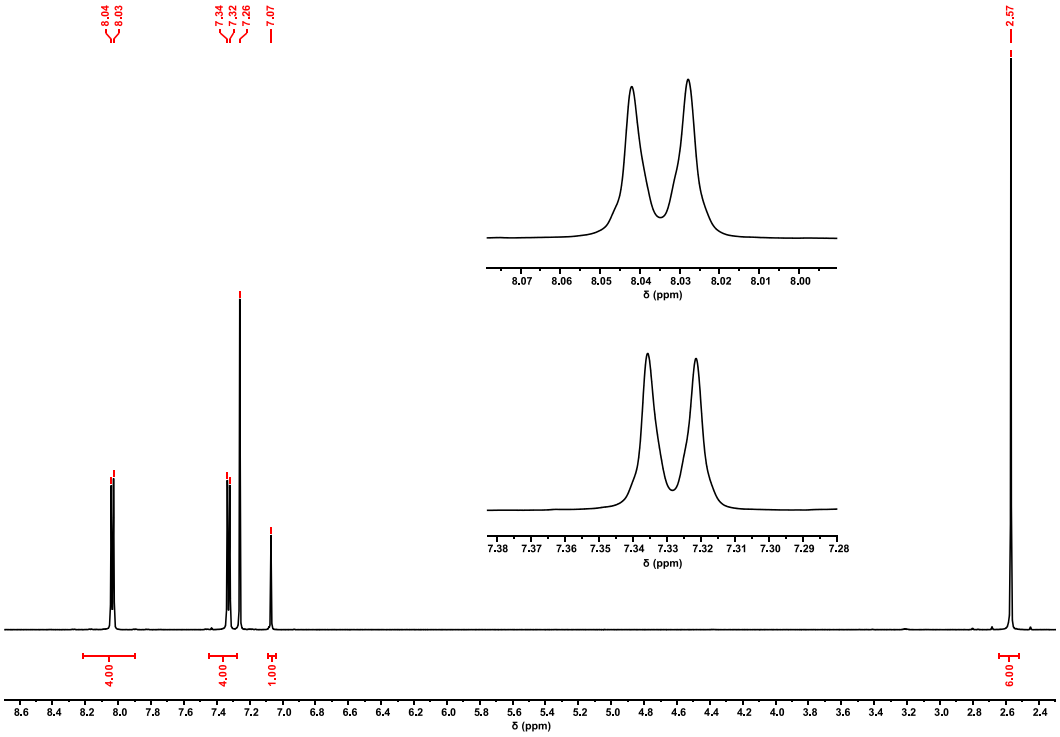

Figure S6 | **^{1}H-NMR** (600 MHz, $CDCl_3$, rt) spectrum of **SMe-BF_2**.

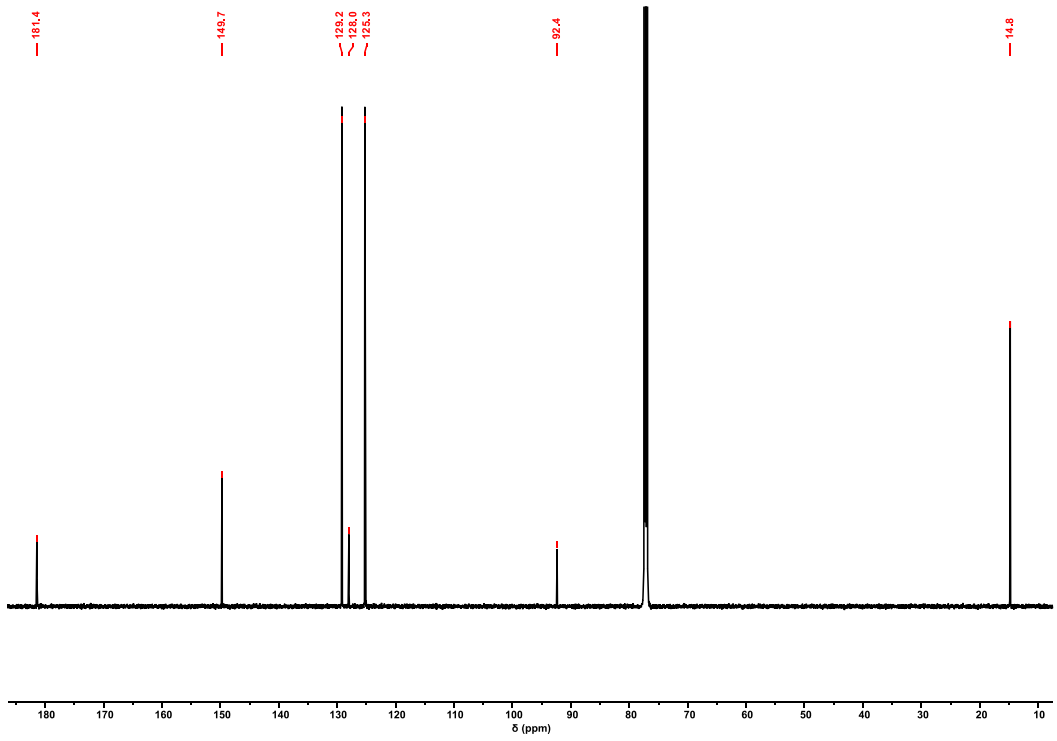

Figure S7 | **^{13}C{^{1}H}-NMR** (151 MHz, $CDCl_3$, rt) spectrum of **SMe-BF_2**.

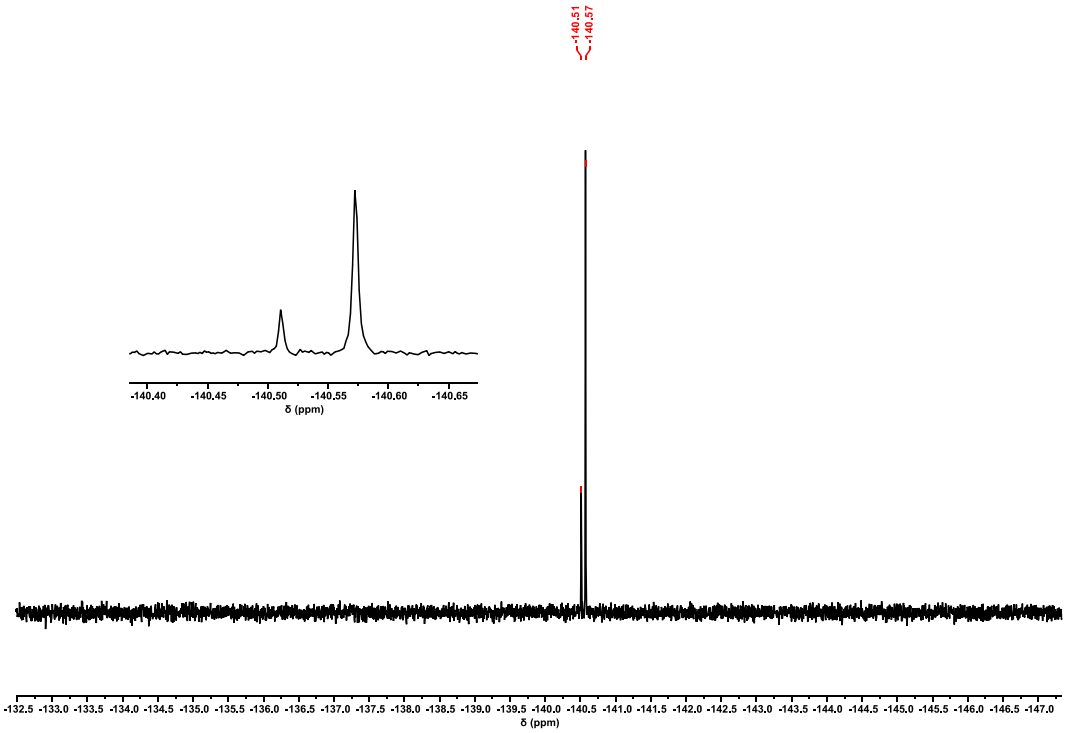

Figure S8 | **^{19}F{^{1}H}-NMR** (376 MHz, $CDCl_3$, rt) spectrum of **SMe-BF$_2$**.

SMe-BPh$^{F}_{2}$

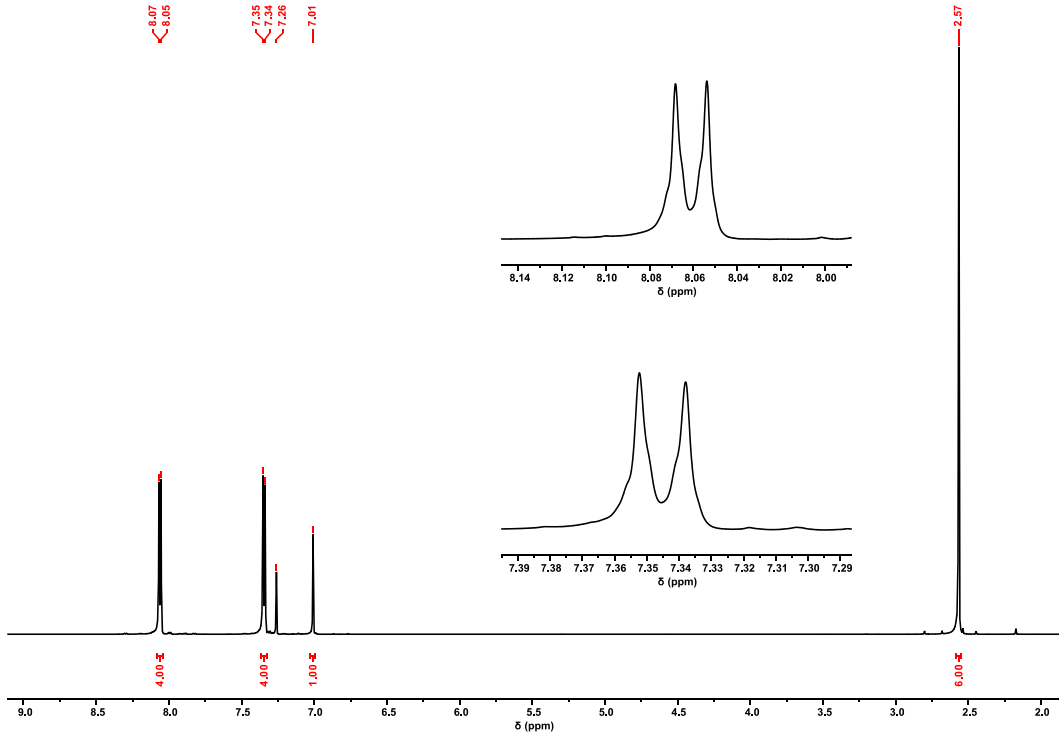

Figure S9 | **^{1}H-NMR** (600 MHz, $CDCl_3$, rt) spectrum of **SMe-BPh$^{F}_{2}$**.

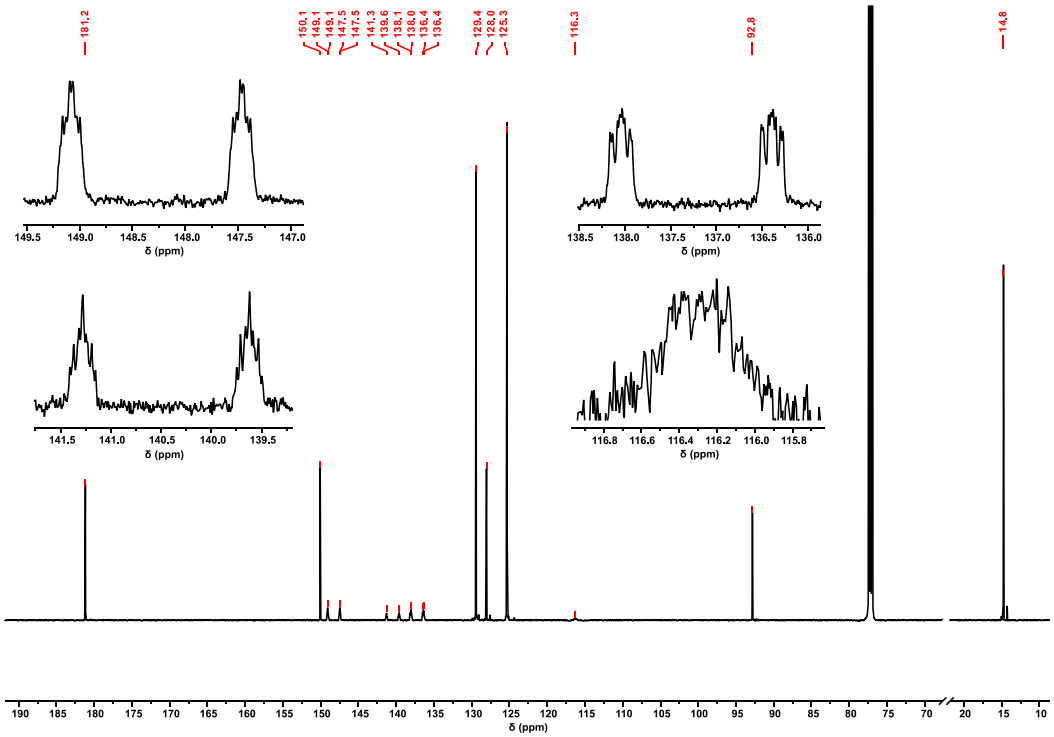

Figure S10 | **$^{13}C\{^{1}H\}$-NMR** (151 MHz, $CDCl_3$, rt) spectrum of **SMe-BPh$^{F}_{2}$**.

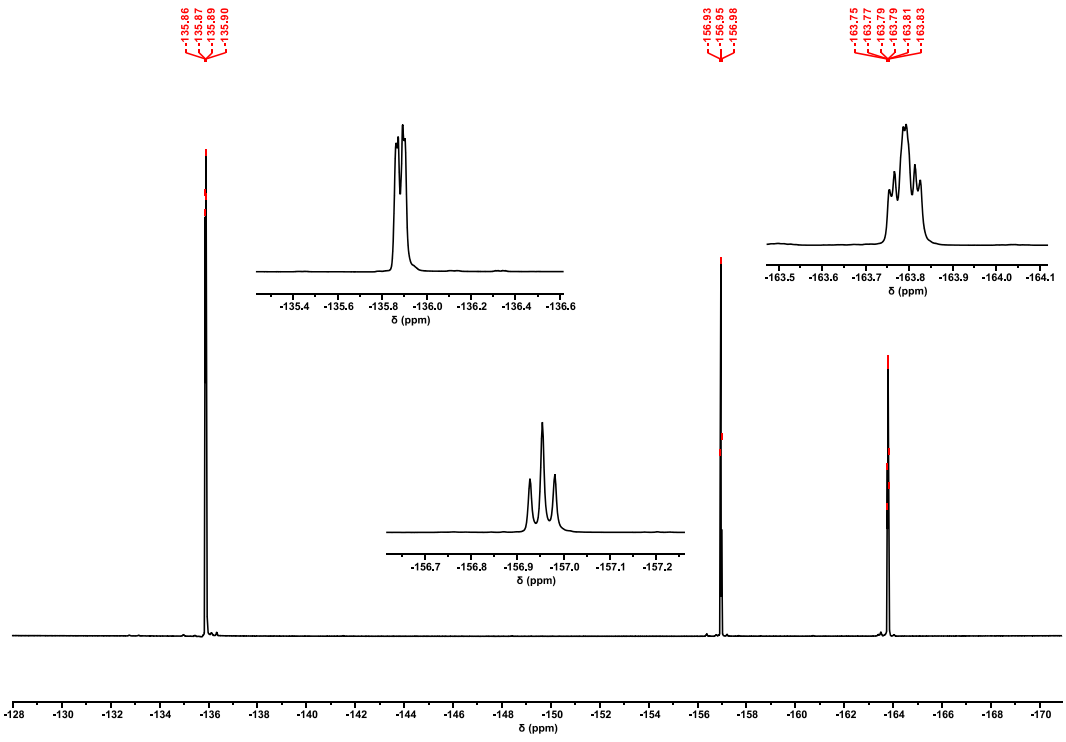

Figure S11 | **$^{19}F\{^{1}H\}$-NMR** (753 MHz, $CDCl_3$, rt) spectrum of **SMe-BPh$^{F}_{2}$**.

SMe-RhCOD

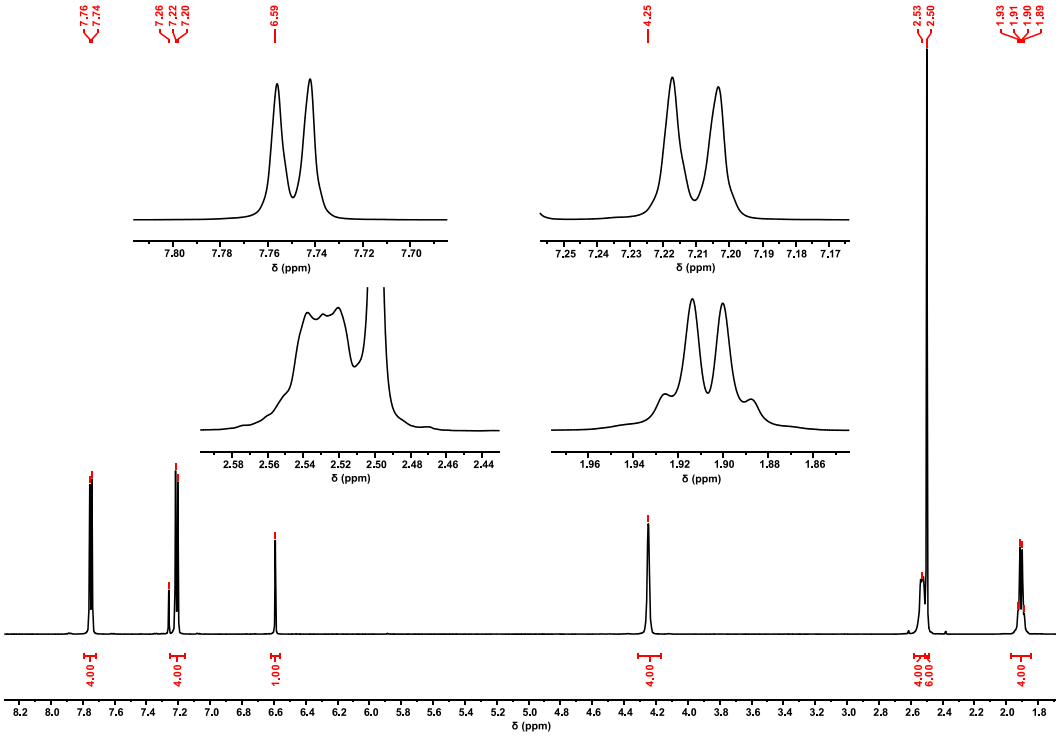

Figure S12 | **^{1}H-NMR** (600 MHz, $CDCl_3$, rt) spectrum of **SMe-RhCOD**.

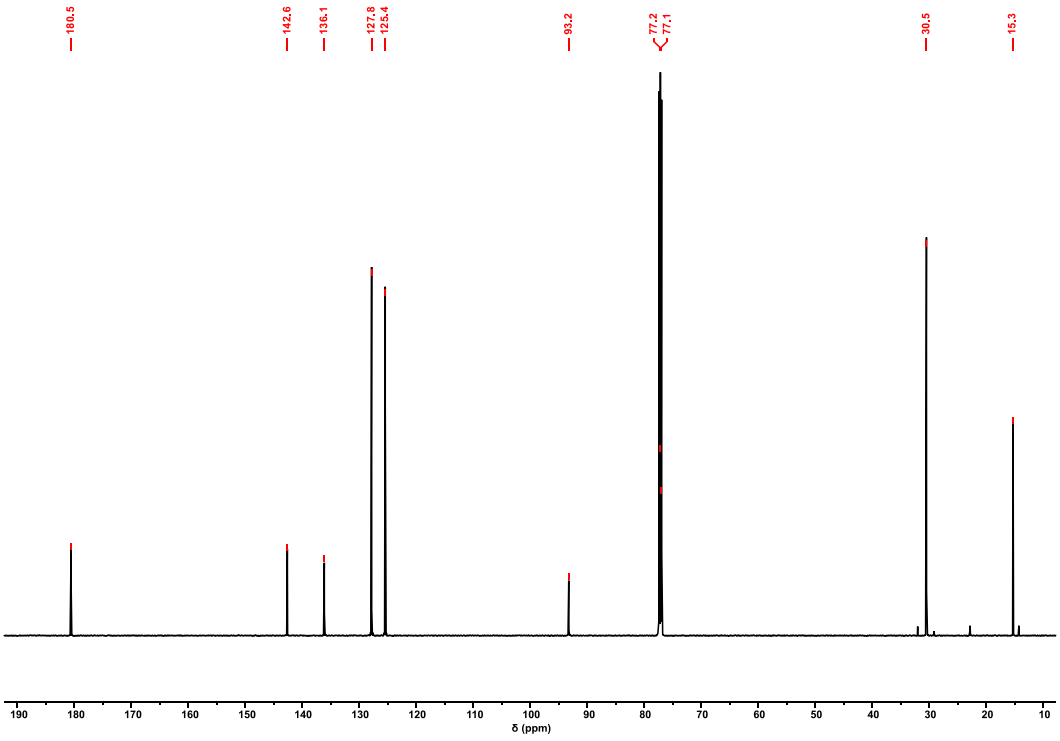

Figure S13 | **^{13}C{^{1}H}-NMR** (151 MHz, $CDCl_3$, rt) spectrum of **SMe-RhCOD**.

SMe-RuP^{i}Pr$_3$

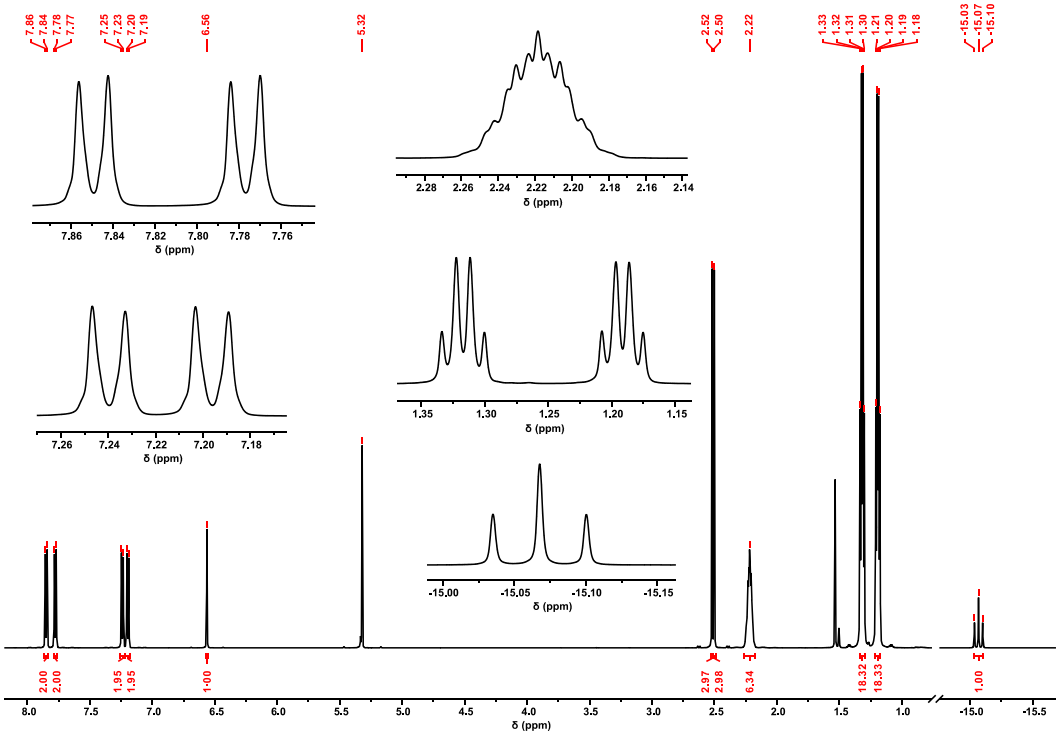

Figure S14 | **^{1}H-NMR** (600 MHz, CD_2Cl_2, rt) spectrum of **SMe-RuP^{i}Pr$_3$**.

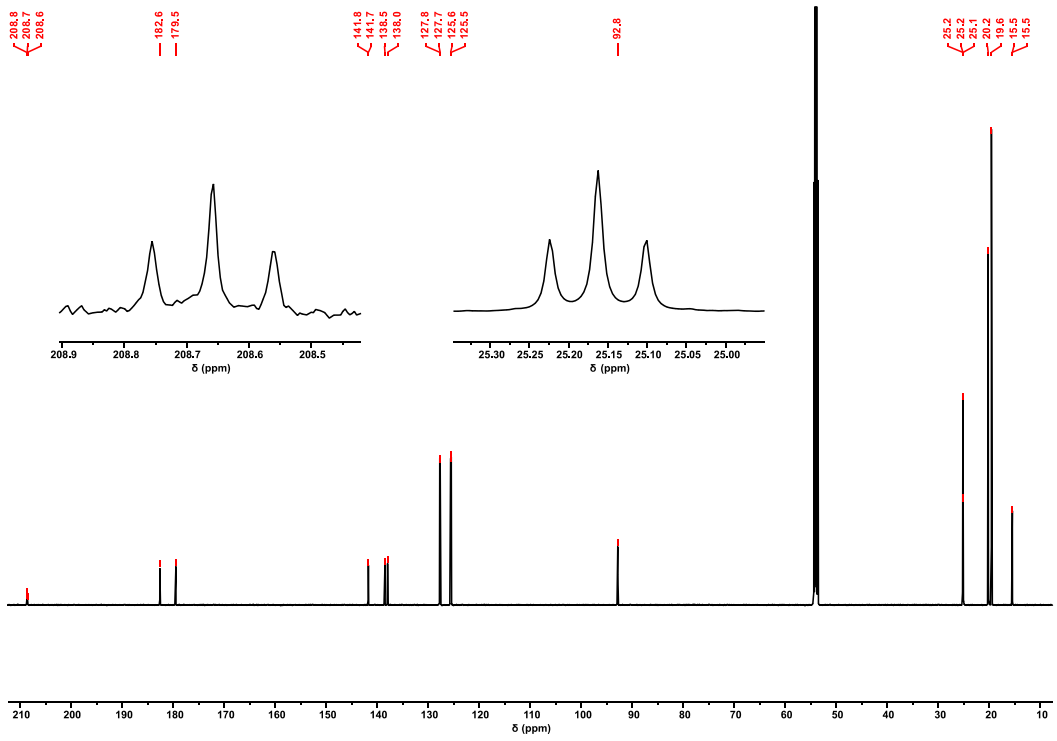

Figure S15 | **^{13}C{^{1}H}-NMR** (151 MHz, CD_2Cl_2, rt) spectrum of **SMe-RuP^{i}Pr$_3$**.

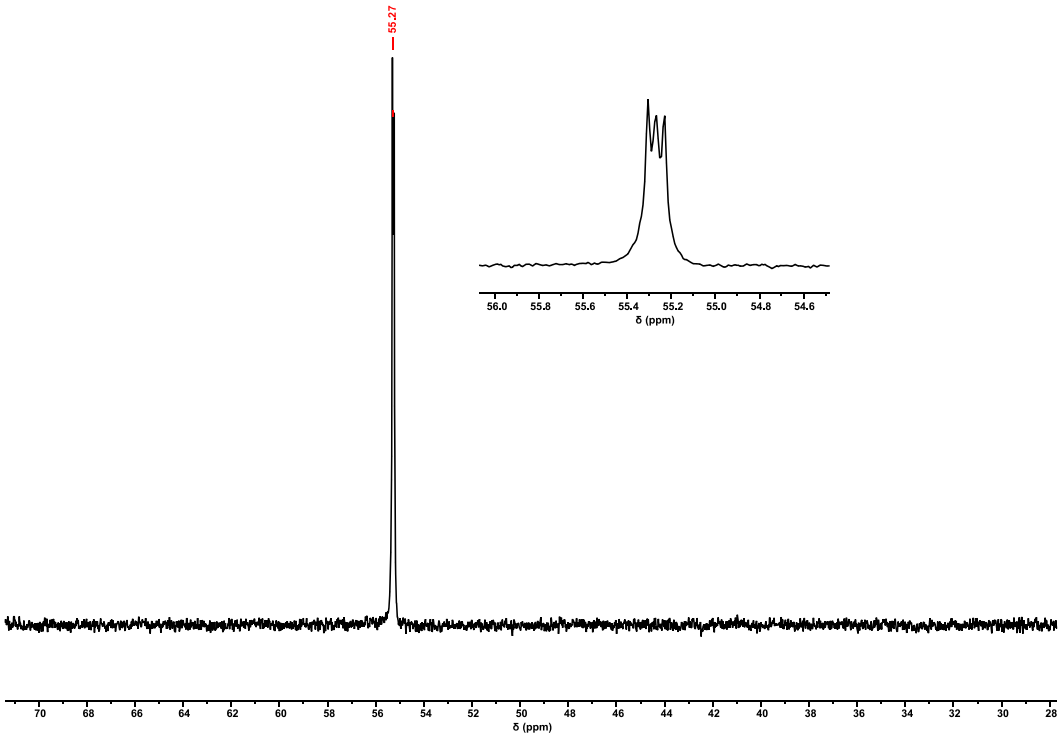

Figure S16 | **$^{31}P\{^{1}H\}$-NMR** (243 MHz, CD_2Cl_2, rt) spectrum of **SMe-RuP^{i}Pr$_3$**.

1SMe-RuP^{i}Pr$_3$

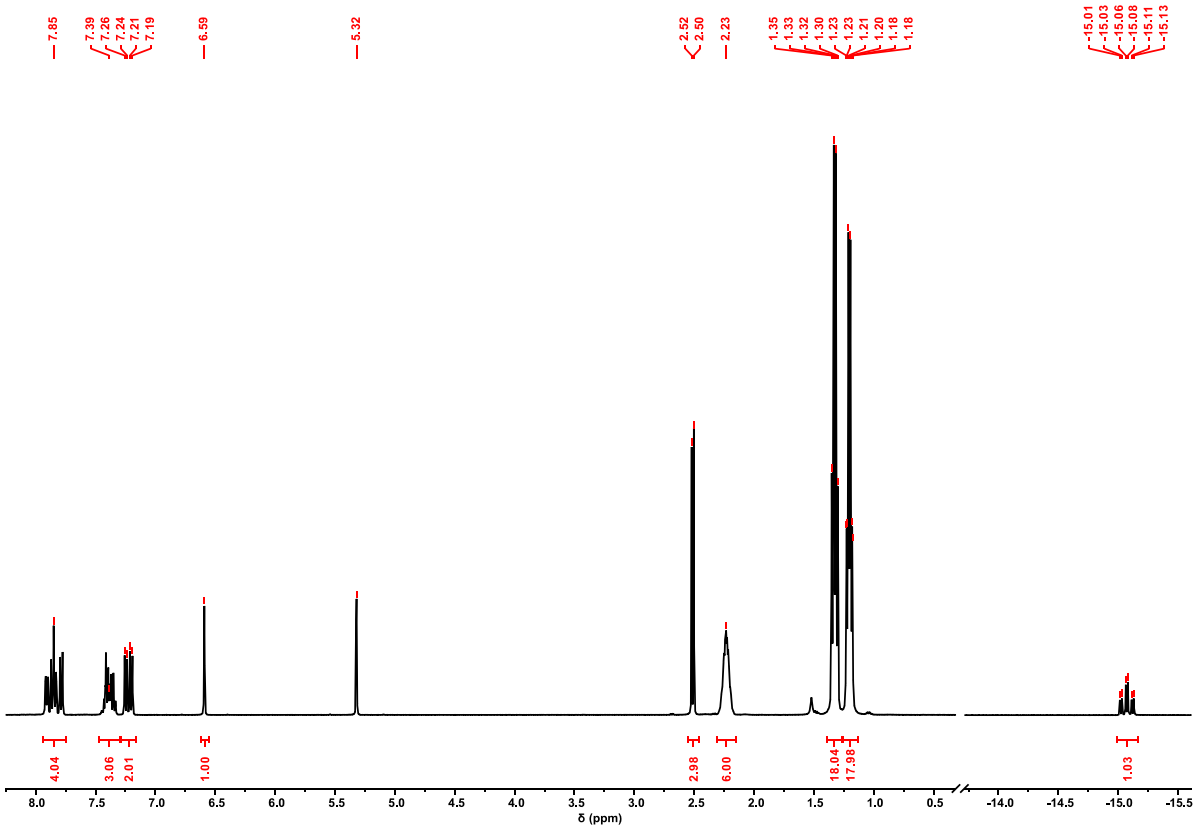

Figure S17 | **^{1}H-NMR** (400 MHz, CD_2Cl_2, rt) spectrum of **1SMe-RuP^{i}Pr$_3$**.

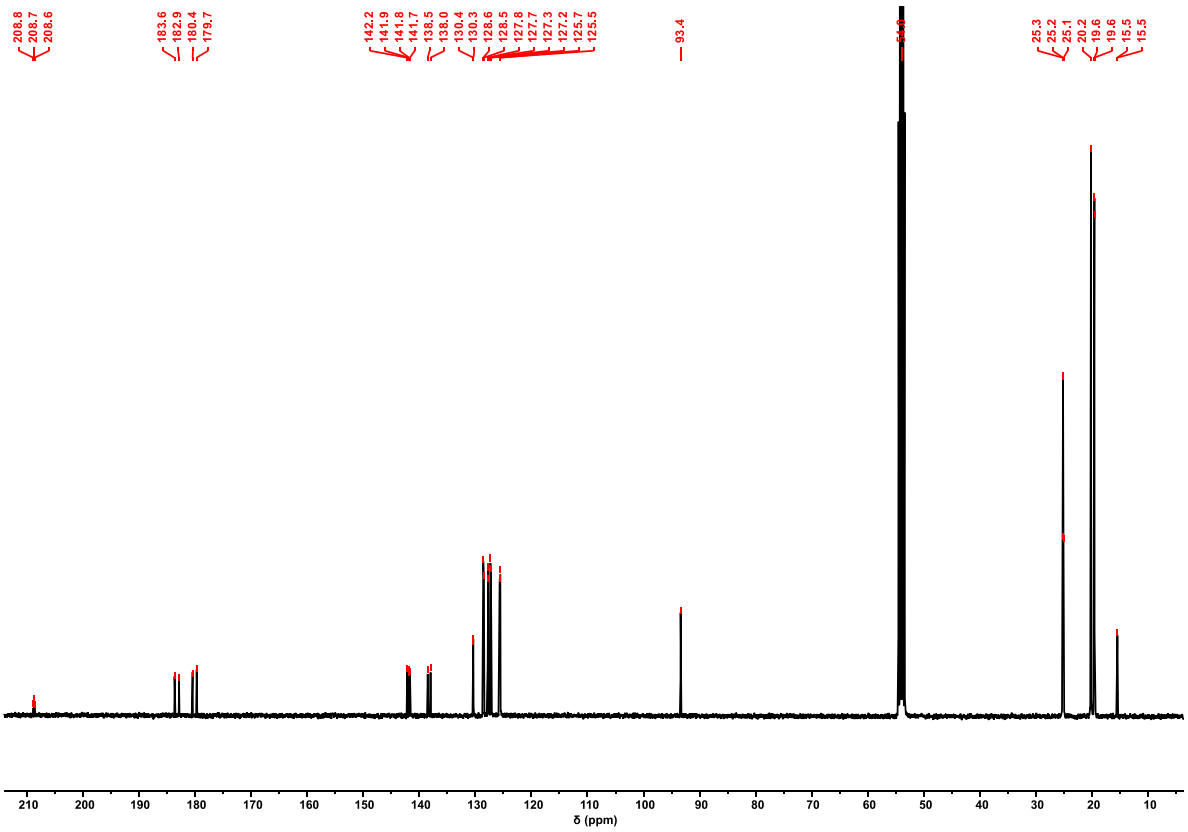

Figure S18 | $^{13}C\{^{1}H\}$-NMR (101 MHz, CD_2Cl_2, rt) spectrum of **1SMe-RuP^{i}Pr$_3$**.

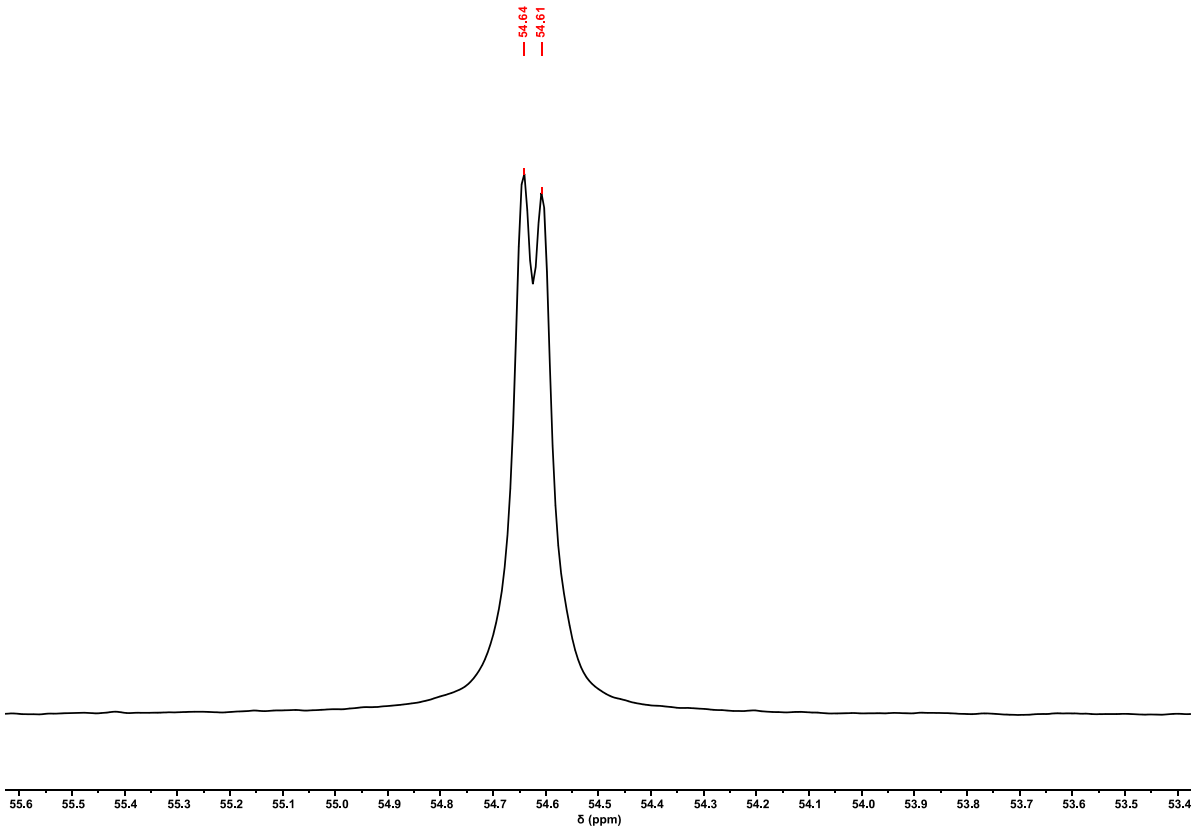

Figure S19 | $^{31}P\{^{1}H\}$-NMR (162 MHz, CD_2Cl_2, rt) spectrum of **1SMe-RuP^{i}Pr$_3$**

SMe-TerPh

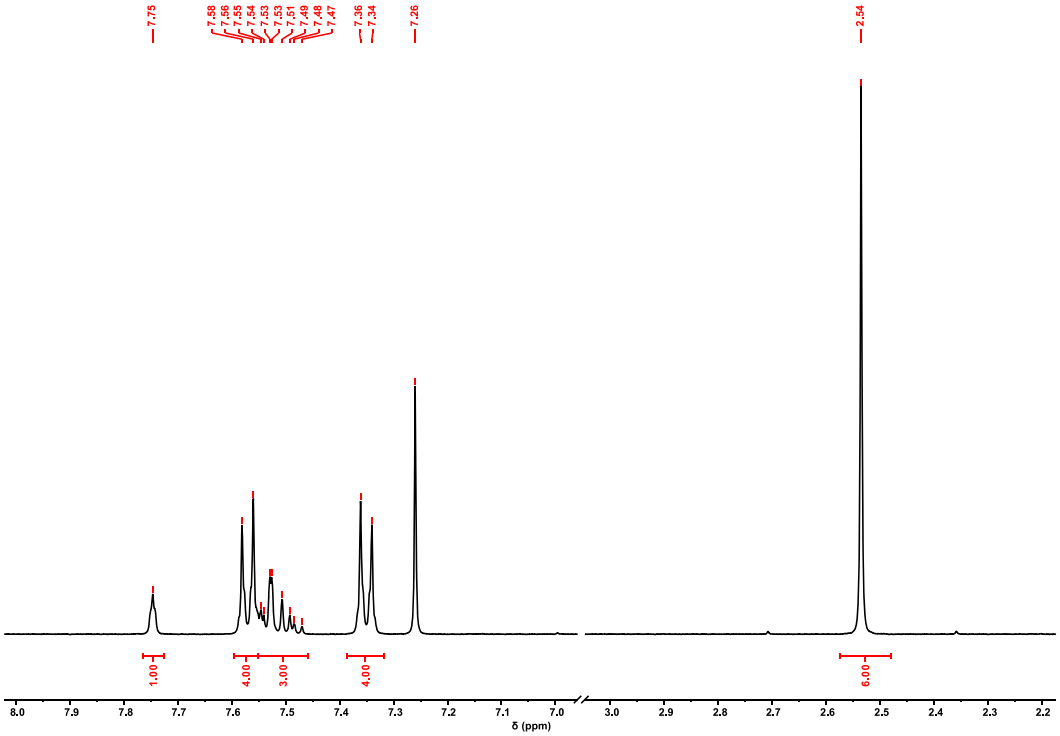

Figure S20 | **^{1}H-NMR** (400 MHz, $CDCl_3$, rt) spectrum of **SMe-TerPh**.

SMe-TerY

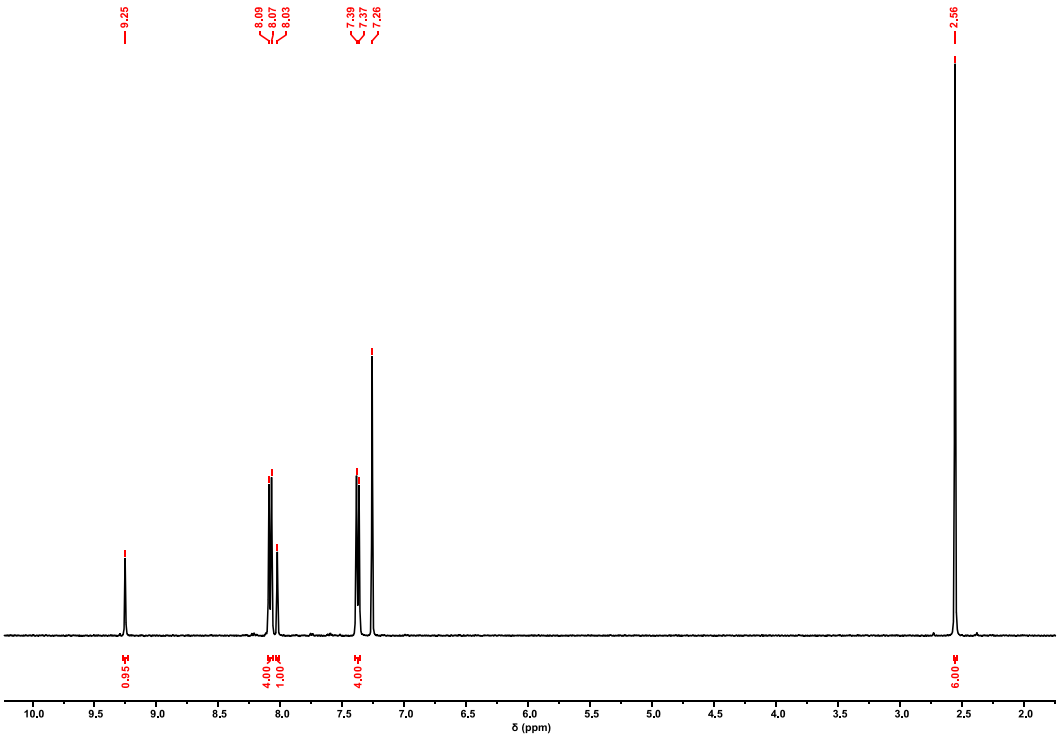

Figure S21 | **^{1}H-NMR** (400 MHz, $CDCl_3$, rt) spectrum of **SMe-TerY**.

Single crystal X-ray diffraction

SMe-H

Single crystals of **SMe-H** were grown by layer diffusion of *n*-pentane into a dichloromethane solution of the compound. The obtained crystallographic information file was submitted to the structural database of The Cambridge Crystallographic Data Centre and can be found under the deposition number CCDC 2161698.

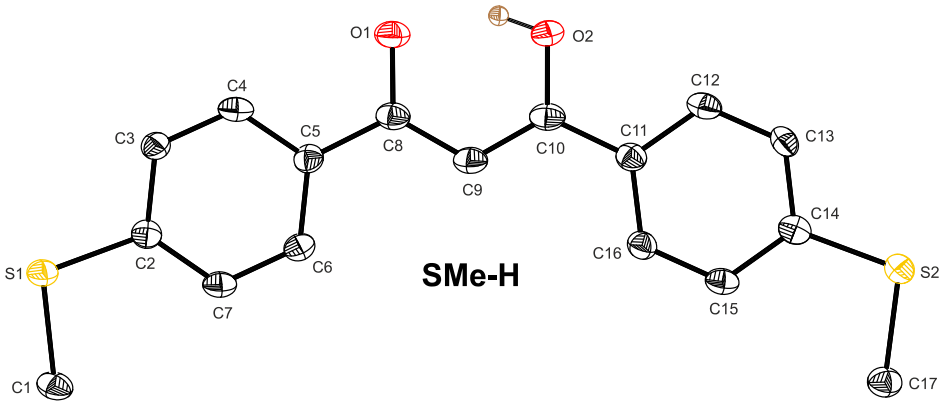

Figure S22 | ORTEP of the free ligand **SMe-H**. Thermal ellipsoids are displayed at a 50% probability level. Hydrogen atoms (except for OH) are omitted for clarity reasons.

Table S3 | Crystal data and structure refinement for **SMe-H**.

Parameter	SMe-H
Empirical formula	$C_{17}H_{16}O_2S_2$
Formula weight	316.42
Temperature (K)	100
Crystal system	orthorhombic
Space group	$P2_12_12_1$
a (Å)	3.9473(2)
b (Å)	11.3841(5)
c (Å)	32.7877(16)
α (°)	90
β (°)	90
γ (°)	90
Volume (Å^3)	1473.36(12)
Z	4
ρ_{calc} (g/cm^3)	1.426
μ (mm^{-1})	0.362
F(000)	664.0
Crystal size (mm^3)	0.1 × 0.1 × 0.1
Radiation	Mo-K_α (λ = 0.71073 Å)
2Θ range for data collection (°)	5.166 to 55.074
Index ranges	$-5 \le h \le 5$, $-12 \le k \le 14$, $-35 \le l \le 42$
Reflections collected	7146
Independent reflections	3334 [R_{int} = 0.0291, R_{sigma} = 0.0323]
Data/restraints/parameters	3334/0/194
Goodness-of-fit on F^2	1.118
Final *R* indexes [$I \ge 2\sigma(I)$]	R_1 = 0.0395, wR_2 = 0.0931
Final *R* indexes [all data]	R_1 = 0.0521, wR_2 = 0.1134
Largest diff. peak/hole (e Å^{-3})	0.35/-0.37
Flack parameter	-0.03(6)

Table S4 | Bond lengths for **SMe-H**.

Atom	Atom	Length (Å)	Atom	Atom	Length (Å)
S1	C1	1.792(4)	C5	C8	1.483(5)
S1	C2	1.750(4)	C6	C7	1.384(5)
S2	C14	1.754(4)	C8	C9	1.401(6)
S2	C17	1.797(4)	C9	C10	1.389(6)
O1	C8	1.284(5)	C10	C11	1.462(6)
O2	C10	1.313(5)	C11	C12	1.401(5)
C2	C3	1.395(5)	C11	C16	1.396(5)
C2	C7	1.398(5)	C12	C13	1.377(6)
C3	C4	1.386(5)	C13	C14	1.395(5)
C4	C5	1.382(5)	C14	C15	1.400(5)
C5	C6	1.399(5)	C15	C16	1.379(6)

Table S5 | Bond angles for **SMe-H**.

Atom	Atom	Atom	Angle (˚)	Atom	Atom	Atom	Angle (˚)
C2	S1	C1	103.61(19)	C10	C9	C8	120.8(4)
C14	S2	C17	103.04(19)	O2	C10	C9	119.6(4)
C3	C2	S1	116.2(3)	O2	C10	C11	115.5(3)
C3	C2	C7	118.5(4)	C9	C10	C11	124.9(4)
C7	C2	S1	125.3(3)	C12	C11	C10	119.4(4)
C4	C3	C2	120.3(4)	C16	C11	C10	122.6(3)
C5	C4	C3	121.5(3)	C16	C11	C12	118.0(4)
C4	C5	C6	118.1(4)	C13	C12	C11	121.0(4)
C4	C5	C8	119.2(3)	C12	C13	C14	120.7(3)
C6	C5	C8	122.7(3)	C13	C14	S2	117.2(3)
C7	C6	C5	120.9(4)	C13	C14	C15	118.7(4)
C6	C7	C2	120.5(4)	C15	C14	S2	124.2(3)
O1	C8	C5	116.2(4)	C16	C15	C14	120.3(4)
O1	C8	C9	120.3(4)	C15	C16	C11	121.3(4)
C9	C8	C5	123.5(3)				

Table S6 | Torsion angles for **SMe-H**.

Atom	Atom	Atom	Atom	Angle (˚)	Atom	Atom	Atom	Atom	Angle (˚)
S1	C2	C3	C4	178.5(3)	C6	C5	C8	C9	-4.3(6)
S1	C2	C7	C6	-177.9(3)	C7	C2	C3	C4	-0.6(6)
S2	C14	C15	C16	-179.5(3)	C8	C5	C6	C7	177.6(4)
O1	C8	C9	C10	2.9(6)	C8	C9	C10	O2	-1.3(6)
O2	C10	C11	C12	-2.0(5)	C8	C9	C10	C11	179.1(4)
O2	C10	C11	C16	179.4(4)	C9	C10	C11	C12	177.5(4)
C1	S1	C2	C3	177.0(3)	C9	C10	C11	C16	-1.0(6)
C1	S1	C2	C7	-3.9(4)	C10	C11	C12	C13	-177.2(4)
C2	C3	C4	C5	-0.9(6)	C10	C11	C16	C15	177.3(4)
C3	C2	C7	C6	1.1(6)	C11	C12	C13	C14	-0.2(6)
C3	C4	C5	C6	2.0(6)	C12	C11	C16	C15	-1.2(6)
C3	C4	C5	C8	-177.1(4)	C12	C13	C14	S2	179.6(3)
C4	C5	C6	C7	-1.4(6)	C12	C13	C14	C15	-1.2(6)
C4	C5	C8	O1	-4.1(6)	C13	C14	C15	C16	1.4(6)
C4	C5	C8	C9	174.7(4)	C14	C15	C16	C11	-0.2(6)
C5	C6	C7	C2	-0.1(6)	C16	C11	C12	C13	1.4(6)
C5	C8	C9	C10	-175.9(4)	C17	S2	C14	C13	-177.1(3)
C6	C5	C8	O1	176.9(4)	C17	S2	C14	C15	3.7(4)

SMe-RhCOD

Single crystals of **SMe-RhCOD** were grown by layer diffusion of *n*-pentane into a dichloromethane solution of the compound. The obtained crystallographic information file was submitted to the structural database of The Cambridge Crystallographic Data Centre and can be found under the deposition number CCDC 2161700.

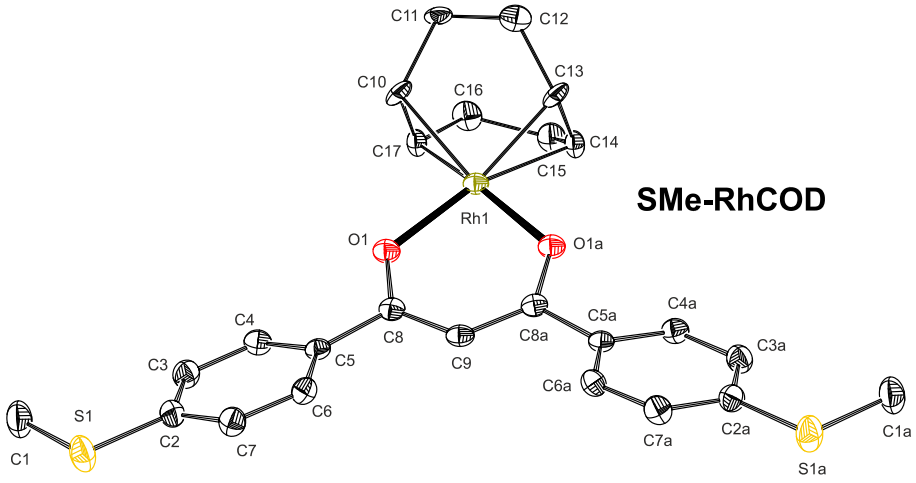

Figure S23 | ORTEP of the DBM based transition metal complex **SMe-RhCOD**. Thermal ellipsoids are displayed at a 50% probability level. Hydrogen atoms, co-crystallized solvent molecules and one part of the COD disorder are omitted for clarity reasons.

Table S7 | Crystal data and structure refinement for **SMe-RhCOD**.

Parameter	SMe-RhCOD
Empirical formula	$C_{25}H_{27}O_2RhS_2$
Formula weight	526.49
Temperature (K)	100.00
Crystal system	orthorhombic
Space group	*Pnma*
a (Å)	9.4517(3)
b (Å)	23.2662(4)
c (Å)	10.4808(7)
α (°)	90
β (°)	90
γ (°)	90
Volume (Å^3)	2304.78(17)
Z	4
ρ_{calc} (g/cm^3)	1.517
μ (mm^{-1})	0.941
F(000)	1080.0
Crystal size (mm^3)	0.3 × 0.15 × 0.1
Radiation	Mo-K_α (λ = 0.71073 Å)
2Θ range for data collection (°)	4.262 to 55.194
Index ranges	-12 ≤ *h* ≤ 11, -25 ≤ *k* ≤ 30, -13 ≤ *l* ≤ 13
Reflections collected	10632
Independent reflections	2723 [R_{int} = 0.0279, R_{sigma} = 0.0211]
Data/restraints/parameters	2723/28/172
Goodness-of-fit on F^2	1.154
Final *R* indexes [$I \geq 2\sigma(I)$]	R_1 = 0.0325, wR_2 = 0.0643
Final *R* indexes [all data]	R_1 = 0.0417, wR_2 = 0.0674
Largest diff. peak/hole (e Å^{-3})	0.33/-0.67

Table S8 | Bond lengths for **SMe-RhCOD**.

Atom	Atom	Length (Å)	Atom	Atom	Length (Å)
Rh1	O1[(a)]	2.0369(17)	C4	C3	1.380(4)
Rh1	O1	2.0369(17)	C3	C2	1.397(4)
Rh1	C10	2.151(16)	C10	C17	1.393(7)
Rh1	C17	2.07(2)	C10	C11	1.508(7)
Rh1	C13	2.068(17)	C6	C7	1.379(4)
Rh1	C14	2.15(2)	C17	C16	1.514(7)
S1	C2	1.760(3)	C2	C7	1.392(4)
S1	C1	1.796(3)	C11	C12	1.531(6)
O1	C8	1.283(3)	C16	C15	1.532(7)
C8	C5	1.482(4)	C12	C13	1.513(7)
C8	C9	1.401(3)	C15	C14	1.521(7)
C5	C4	1.394(4)	C13	C14	1.391(7)
C5	C6	1.400(3)			

(a) +X, 1/2-Y, +Z.

Table S9 | Bond angles for **SMe-RhCOD**.

Atom	Atom	Atom	Angle (˚)	Atom	Atom	Atom	Angle (˚)
O1[(a)]	Rh1	O1	91.16(10)	C4	C3	C2	120.0(3)
O1[(a)]	Rh1	C10	161.1(3)	C17	C10	Rh1	67.7(11)
O1	Rh1	C10	91.8(3)	C17	C10	C11	115.2(11)
O1	Rh1	C17	93.5(3)	C11	C10	Rh1	112.2(8)
O1[(a)]	Rh1	C17	159.7(3)	C7	C6	C5	120.5(2)
O1	Rh1	C13	160.5(3)	C10	C17	Rh1	73.8(10)
O1[(a)]	Rh1	C13	88.7(3)	C10	C17	C16	120.5(9)
O1	Rh1	C14	160.9(3)	C16	C17	Rh1	115.2(12)
O1[(a)]	Rh1	C14	86.2(2)	C8	C9	C8[(a)]	127.1(3)
C17	Rh1	C10	38.4(3)	C3	C2	S1	124.4(2)
C17	Rh1	C14	82.9(2)	C7	C2	S1	117.1(2)
C13	Rh1	C10	82.39(17)	C7	C2	C3	118.6(2)
C13	Rh1	C17	93.4(5)	C6	C7	C2	121.3(2)
C13	Rh1	C14	38.5(3)	C10	C11	C12	110.8(9)
C14	Rh1	C10	96.8(4)	C17	C16	C15	110.8(13)
C2	S1	C1	102.96(14)	C13	C12	C11	112.7(10)
C8	O1	Rh1	125.42(17)	C14	C15	C16	115.0(11)
O1	C8	C5	114.1(2)	C12	C13	Rh1	110.1(8)
O1	C8	C9	125.4(3)	C14	C13	Rh1	73.8(11)
C9	C8	C5	120.5(2)	C14	C13	C12	135.7(12)
C4	C5	C8	119.7(2)	C15	C14	Rh1	107.8(12)
C4	C5	C6	118.0(2)	C13	C14	Rh1	67.7(11)
C6	C5	C8	122.2(2)	C13	C14	C15	128.1(9)
C3	C4	C5	121.6(2)				

(a) +X, 1/2-Y, +Z.

Table S10 | Torsion angles for **SMe-RhCOD**.

Atom	Atom	Atom	Atom	Angle (˚)	Atom	Atom	Atom	Atom	Angle (˚)
Rh1	O1	C8	C5	-178.53(15)	C3	C2	C7	C6	0.7(4)
Rh1	O1	C8	C9	1.2(4)	C10	C17	C16	C15	95(2)
Rh1	C10	C17	C16	-110.1(18)	C10	C11	C12	C13	34.5(14)
Rh1	C10	C11	C12	-15.1(11)	C6	C5	C4	C3	1.4(4)
Rh1	C17	C16	C15	9.4(10)	C17	C10	C11	C12	-90.0(17)
Rh1	C13	C14	C15	96(2)	C17	C16	C15	C14	-27.7(13)
S1	C2	C7	C6	-178.6(2)	C9	C8	C5	C4	-156.5(3)
O1	C8	C5	C4	23.3(3)	C9	C8	C5	C6	26.7(4)
O1	C8	C5	C6	-153.5(2)	C1	S1	C2	C3	-7.3(3)
O1	C8	C9	C8[(a)]	-1.2(6)	C1	S1	C2	C7	172.0(2)
C8	C5	C4	C3	-175.5(2)	C11	C10	C17	Rh1	105.0(12)
C8	C5	C6	C7	174.4(2)	C11	C10	C17	C16	-5(3)
C5	C8	C9	C8[(a)]	178.5(2)	C11	C12	C13	Rh1	-37.7(10)
C5	C4	C3	C2	0.6(4)	C11	C12	C13	C14	49(3)
C5	C6	C7	C2	1.3(4)	C16	C15	C14	Rh1	31.8(10)
C4	C5	C6	C7	-2.4(4)	C16	C15	C14	C13	-43(3)
C4	C3	C2	S1	177.6(2)	C12	C13	C14	Rh1	-102(2)
C4	C3	C2	C7	-1.7(4)	C12	C13	C14	C15	-7(4)

(a) +X, 1/2-Y, +Z.

SMe-RuP^{i}Pr$_3$

Single crystals of **SMe-RuP^{i}Pr$_3$** were grown by layer diffusion of *n*-pentane into a dichloromethane solution of the compound. The obtained crystallographic information file was submitted to the structural database of The Cambridge Crystallographic Data Centre and can be found under the deposition number CCDC 2161701.

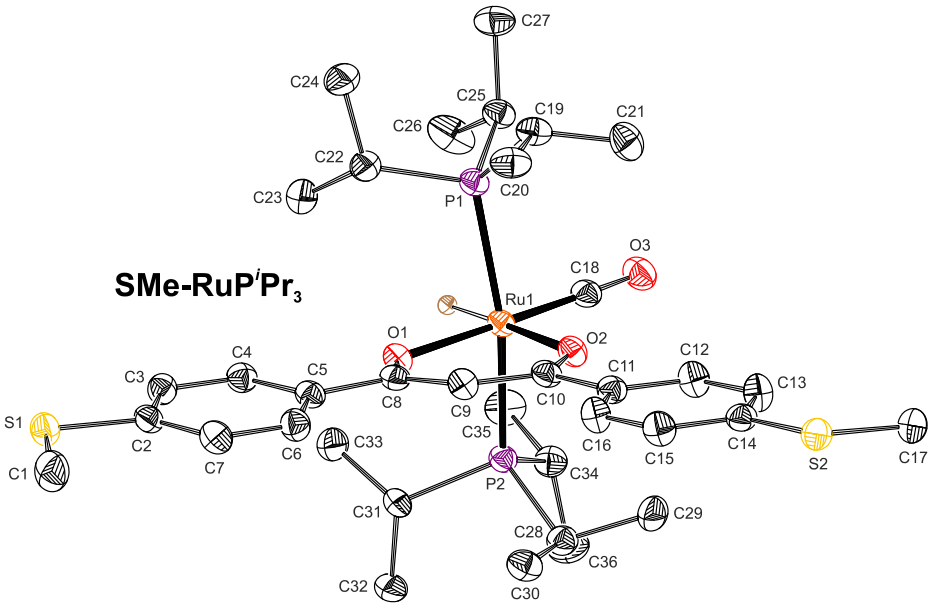

Figure S24 | ORTEPs of the transition metal complex **SMe-RuP^{i}Pr$_3$**. Thermal ellipsoids are displayed at a 50% probability level. Hydrogen atoms (except for RuH) and co-crystallized solvent molecules are omitted for clarity reasons.

Table S11 | Crystal data and structure refinement for **SMe-RuP^{i}Pr$_3$ · CH$_2$Cl$_2$**.

Parameter	SMe-RuP^{i}Pr$_3$ · CH$_2$Cl$_2$
Empirical formula	$C_{37}H_{60}Cl_2O_3P_2RuS_2$
Formula weight	850.88
Temperature (K)	100
Crystal system	triclinic
Space group	$P\bar{1}$
a (Å)	9.9782(4)
b (Å)	12.4346(5)
c (Å)	17.8296(7)
α (°)	73.003(3)
β (°)	80.029(3)
γ (°)	78.029(3)
Volume (Å^3)	2054.55(15)
Z	2
ρ_{calc} (g/cm^3)	1.375
M (mm^{-1})	0.724
F(000)	892.0
Crystal size (mm^3)	0.4 × 0.267 × 0.1
Radiation	Mo-K$_\alpha$ (λ = 0.71073 Å)
2Θ range for data collection (°)	3.474 to 58.488
Index ranges	-13 ≤ *h* ≤ 13, -17 ≤ *k* ≤ 17, -22 ≤ *l* ≤ 24
Reflections collected	34768
Independent reflections	11072 [R_{int} = 0.0629, R_{sigma} = 0.0485]
Data/restraints/parameters	11072/0/443
Goodness-of-fit on F^2	1.049
Final *R* indexes [$I \geq 2\sigma(I)$]	R_1 = 0.0477, wR_2 = 0.1262
Final *R* indexes [all data]	R_1 = 0.0605, wR_2 = 0.1334
Largest diff. peak/hole (e Å^{-3})	0.85/-1.23

Table S12 | Bond lengths for **SMe-RuP^{i}Pr$_3$ · CH$_2$Cl$_2$**.

Atom	Atom	Length (Å)	Atom	Atom	Length (Å)
Ru1	P1	2.3780(7)	C6	C7	1.386(4)
Ru1	P2	2.3814(6)	C8	C9	1.407(3)
Ru1	O1	2.1319(18)	C9	C10	1.409(4)
Ru1	O2	2.1864(17)	C10	C11	1.501(3)
Ru1	C18	1.805(3)	C11	C12	1.386(4)
S1	C1	1.794(3)	C11	C16	1.404(4)
S1	C2	1.762(3)	C12	C13	1.386(4)
S2	C14	1.757(3)	C13	C14	1.394(4)
S2	C17	1.797(3)	C14	C15	1.394(4)
P1	C19	1.860(3)	C15	C16	1.377(4)
P1	C22	1.862(3)	C19	C20	1.530(4)
P1	C25	1.869(3)	C19	C21	1.528(4)
P2	C28	1.855(3)	C22	C23	1.534(4)
P2	C31	1.857(3)	C22	C24	1.537(4)
P2	C34	1.869(3)	C25	C26	1.523(4)
O1	C8	1.277(3)	C25	C27	1.530(4)
O2	C10	1.263(3)	C28	C29	1.542(4)
O3	C18	1.162(3)	C28	C30	1.535(4)
C2	C3	1.403(4)	C31	C32	1.528(3)
C2	C7	1.386(4)	C31	C33	1.542(4)
C3	C4	1.383(4)	C34	C35	1.530(4)
C4	C5	1.402(3)	C34	C36	1.535(4)
C5	C6	1.386(4)	Cl1	C37	1.730(4)
C5	C8	1.499(3)	Cl2	C37	1.693(5)

Table S13 | Bond angles for **SMe-RuP^{i}Pr$_3$ · CH_2Cl_2**.

Atom	Atom	Atom	Angle (˚)	Atom	Atom	Atom	Angle (˚)
P1	Ru1	P2	165.23(2)	O1	C8	C9	125.9(2)
O1	Ru1	P1	90.14(5)	C9	C8	C5	119.2(2)
O1	Ru1	P2	88.52(5)	C8	C9	C10	126.3(2)
O1	Ru1	O2	84.49(7)	O2	C10	C9	125.3(2)
O2	Ru1	P1	97.84(5)	O2	C10	C11	115.5(2)
O2	Ru1	P2	96.68(5)	C9	C10	C11	119.2(2)
C18	Ru1	P1	90.05(8)	C12	C11	C10	118.6(2)
C18	Ru1	P2	90.67(8)	C12	C11	C16	117.1(2)
C18	Ru1	O1	177.50(9)	C16	C11	C10	124.3(2)
C18	Ru1	O2	97.96(9)	C13	C12	C11	122.4(3)
C2	S1	C1	103.67(14)	C12	C13	C14	119.9(3)
C14	S2	C17	103.80(13)	C13	C14	S2	124.8(2)
C19	P1	Ru1	118.29(9)	C13	C14	C15	118.2(2)
C19	P1	C22	102.89(12)	C15	C14	S2	117.0(2)
C19	P1	C25	100.98(12)	C16	C15	C14	121.3(3)
C22	P1	Ru1	111.59(8)	C15	C16	C11	120.9(3)
C22	P1	C25	110.05(12)	O3	C18	Ru1	178.4(2)
C25	P1	Ru1	112.17(9)	C20	C19	P1	112.76(19)
C28	P2	Ru1	119.21(8)	C21	C19	P1	110.57(19)
C28	P2	C31	102.54(12)	C21	C19	C20	110.5(2)
C28	P2	C34	101.24(12)	C23	C22	P1	113.50(19)
C31	P2	Ru1	110.91(8)	C23	C22	C24	109.8(2)
C31	P2	C34	110.03(12)	C24	C22	P1	117.1(2)
C34	P2	Ru1	112.09(9)	C26	C25	P1	114.00(19)
C8	O1	Ru1	129.08(16)	C26	C25	C27	109.0(2)
C10	O2	Ru1	128.54(16)	C27	C25	P1	116.87(19)
C3	C2	S1	116.25(19)	C29	C28	P2	110.07(19)
C7	C2	S1	124.8(2)	C30	C28	P2	113.13(19)
C7	C2	C3	119.0(2)	C30	C28	C29	110.5(2)
C4	C3	C2	120.2(2)	C32	C31	P2	115.15(19)
C3	C4	C5	121.1(2)	C32	C31	C33	109.7(2)
C4	C5	C8	119.0(2)	C33	C31	P2	113.78(18)
C6	C5	C4	117.6(2)	C35	C34	P2	113.35(19)
C6	C5	C8	123.4(2)	C35	C34	C36	109.5(2)
C7	C6	C5	121.9(2)	C36	C34	P2	117.6(2)
C2	C7	C6	120.1(3)	Cl2	C37	Cl1	116.0(3)
O1	C8	C5	114.9(2)				

Table S14 | Torsion angles for **SMe-RuP^{i}Pr$_3$ · CH$_2$Cl$_2$**.

Atom	Atom	Atom	Atom	Angle (˚)	Atom	Atom	Atom	Atom	Angle (˚)
Ru1	P1	C19	C20	-70.1(2)	C8	C9	C10	C11	-175.0(2)
Ru1	P1	C19	C21	54.1(2)	C9	C10	C11	C12	-179.9(2)
Ru1	P1	C22	C23	-57.0(2)	C9	C10	C11	C16	0.1(4)
Ru1	P1	C22	C24	173.42(19)	C10	C11	C12	C13	-180.0(2)
Ru1	P1	C25	C26	59.0(2)	C10	C11	C16	C15	179.8(2)
Ru1	P1	C25	C27	-172.28(18)	C11	C12	C13	C14	-0.2(4)
Ru1	P2	C28	C29	-55.4(2)	C12	C11	C16	C15	-0.2(4)
Ru1	P2	C28	C30	68.8(2)	C12	C13	C14	S2	-178.3(2)
Ru1	P2	C31	C32	176.36(17)	C12	C13	C14	C15	0.5(4)
Ru1	P2	C31	C33	48.4(2)	C13	C14	C15	C16	-0.6(4)
Ru1	P2	C34	C35	-59.9(2)	C14	C15	C16	C11	0.5(4)
Ru1	P2	C34	C36	170.55(19)	C16	C11	C12	C13	0.0(4)
Ru1	O1	C8	C5	176.35(14)	C17	S2	C14	C13	-7.5(3)
Ru1	O1	C8	C9	-3.8(4)	C17	S2	C14	C15	173.6(2)
Ru1	O2	C10	C9	-1.1(4)	C19	P1	C22	C23	175.12(19)
Ru1	O2	C10	C11	179.03(14)	C19	P1	C22	C24	45.6(2)
S1	C2	C3	C4	178.95(19)	C19	P1	C25	C26	-174.1(2)
S1	C2	C7	C6	-178.3(2)	C19	P1	C25	C27	-45.4(2)
S2	C14	C15	C16	178.2(2)	C22	P1	C19	C20	53.4(2)
O1	C8	C9	C10	-2.6(4)	C22	P1	C19	C21	177.63(19)
O2	C10	C11	C12	-0.1(3)	C22	P1	C25	C26	-65.9(2)
O2	C10	C11	C16	180.0(2)	C22	P1	C25	C27	62.8(2)
C1	S1	C2	C3	178.2(2)	C25	P1	C19	C20	167.2(2)
C1	S1	C2	C7	-2.3(3)	C25	P1	C19	C21	-68.6(2)
C2	C3	C4	C5	-1.0(4)	C25	P1	C22	C23	68.2(2)
C3	C2	C7	C6	1.1(4)	C25	P1	C22	C24	-61.4(2)
C3	C4	C5	C6	2.0(4)	C28	P2	C31	C32	-55.3(2)
C3	C4	C5	C8	-177.5(2)	C28	P2	C31	C33	176.8(2)
C4	C5	C6	C7	-1.4(4)	C28	P2	C34	C35	171.9(2)
C4	C5	C8	O1	-8.2(3)	C28	P2	C34	C36	42.4(2)
C4	C5	C8	C9	172.0(2)	C31	P2	C28	C29	-178.32(19)
C5	C6	C7	C2	-0.1(4)	C31	P2	C28	C30	-54.1(2)
C5	C8	C9	C10	177.3(2)	C31	P2	C34	C35	64.0(2)
C6	C5	C8	O1	172.4(2)	C31	P2	C34	C36	-65.5(2)
C6	C5	C8	C9	-7.4(4)	C34	P2	C28	C29	68.0(2)
C7	C2	C3	C4	-0.6(4)	C34	P2	C28	C30	-167.81(19)
C8	C5	C6	C7	178.0(2)	C34	P2	C31	C32	51.8(2)
C8	C9	C10	O2	5.2(4)	C34	P2	C31	C33	-76.1(2)

SMe-BPh$^F_2$

Single crystals of **SMe-BPh$^F_2$** were grown by slow evaporation of a *n*-heptane solution of the compound. The obtained crystallographic information file was submitted to the structural database of The

Cambridge Crystallographic Data Centre and can be found under the deposition number CCDC 2161703.

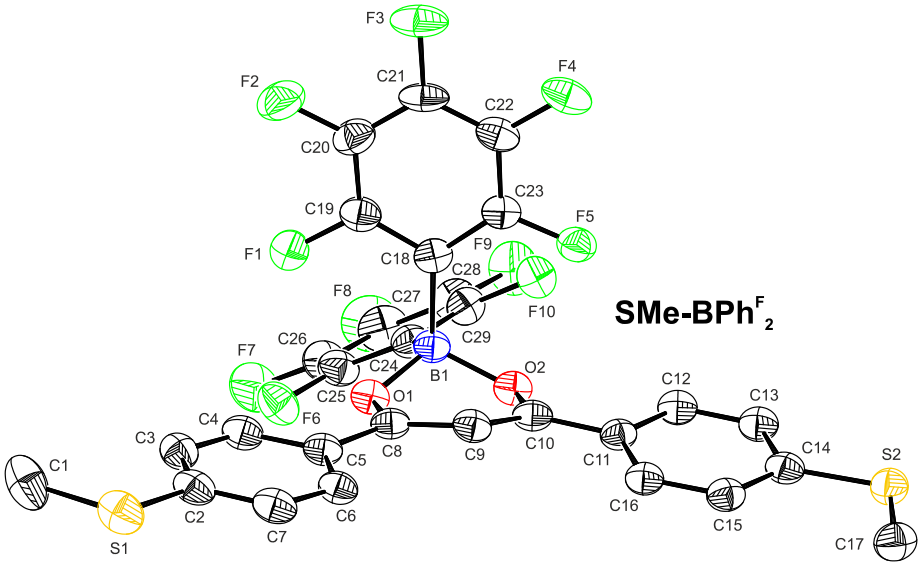

Figure S25 | ORTEP of the coordination compound **SMe-BPh$^{F}_{2}$**. Thermal ellipsoids are displayed at a 50% probability level. Hydrogen atoms, the second molecular entity within the cell and co-crystallized solvent molecules are omitted for clarity reasons.

Table S15 | Crystal data and structure refinement for **$(SMe\text{-}BPh^{F}_{2})_2 \cdot C_7H_{16}$**.

Parameter	$(SMe\text{-}BPh^{F}_{2})_2 \cdot C_7H_{16}$
Empirical formula	$C_{65}H_{46}B_2F_{20}O_4S_4$
Formula weight	1420.88
Temperature (K)	100
Crystal system	monoclinic
Space group	$P2_1/n$
a (Å)	8.7932(6)
b (Å)	21.5764(9)
c (Å)	32.252(2)
α (°)	90
β (°)	95.172(5)
γ (°)	90
Volume (Å^3)	6094.1(7)
Z	4
ρ_{calc} (g/cm^3)	1.549
μ (mm^{-1})	0.268
F(000)	2888.0
Crystal size (mm^3)	0.4 × 0.233 × 0.1
Radiation	Mo-K_α (λ = 0.71073 Å)
2Θ range for data collection (°)	3.776 to 56.732
Index ranges	$-10 \le h \le 11$, $-28 \le k \le 26$, $-43 \le l \le 43$
Reflections collected	53375
Independent reflections	15200 [R_{int} = 0.0919, R_{sigma} = 0.1129]
Data/restraints/parameters	15200/210/928
Goodness-of-fit on F^2	0.828
Final *R* indexes [$I \ge 2\sigma(I)$]	R_1 = 0.0515, wR_2 = 0.0978
Final *R* indexes [all data]	R_1 = 0.1484, wR_2 = 0.1244
Largest diff. peak/hole (e Å^{-3})	0.34/-0.31

Table S16 | Bond lengths for **(SMe-BPh$^{F}_{2}$)$_2$ · C$_7$H$_{16}$**.

Atom	Atom	Length (Å)	Atom	Atom	Length (Å)
S1	C1	1.782(4)	F13	C50	1.345(4)
S1	C2	1.744(3)	F14	C51	1.353(4)
S2	C14	1.749(3)	F15	C52	1.358(3)
S2	C17	1.794(3)	F16	C54	1.357(3)
F1	C19	1.359(3)	F17	C55	1.356(4)
F2	C20	1.347(4)	F18	C56	1.352(4)
F3	C21	1.353(3)	F19	C57	1.346(4)
F4	C22	1.346(3)	F20	C58	1.350(3)
F5	C23	1.351(3)	O3	C37	1.323(3)
F6	C25	1.355(4)	O3	B2	1.499(4)
F7	C26	1.348(4)	O4	C39	1.316(3)
F8	C27	1.347(3)	O4	B2	1.491(4)
F9	C28	1.349(4)	C31	C32	1.411(4)
F10	C29	1.349(3)	C31	C36	1.402(4)
O1	C8	1.313(3)	C32	C33	1.377(4)
O1	B1	1.499(4)	C33	C34	1.403(4)
O2	C10	1.321(3)	C34	C35	1.401(4)
O2	B1	1.502(4)	C34	C37	1.460(4)
C2	C3	1.403(4)	C35	C36	1.379(4)
C2	C7	1.398(4)	C37	C38	1.384(4)
C3	C4	1.381(4)	C38	C39	1.391(4)
C4	C5	1.394(4)	C39	C40	1.465(4)
C5	C6	1.408(4)	C40	C41	1.381(4)
C5	C8	1.456(4)	C40	C45	1.411(4)
C6	C7	1.369(4)	C41	C42	1.384(4)
C8	C9	1.397(4)	C42	C43	1.402(4)
C9	C10	1.391(4)	C43	C44	1.400(5)
C10	C11	1.460(4)	C44	C45	1.380(4)
C11	C12	1.405(4)	C47	C48	1.386(4)
C11	C16	1.401(4)	C47	C52	1.392(4)
C12	C13	1.373(4)	C47	B2	1.643(4)
C13	C14	1.400(4)	C48	C49	1.380(4)
C14	C15	1.405(4)	C49	C50	1.372(5)
C15	C16	1.377(4)	C50	C51	1.373(5)
C18	C19	1.388(4)	C51	C52	1.370(4)
C18	C23	1.386(4)	C53	C54	1.384(4)
C18	B1	1.642(5)	C53	C58	1.389(4)
C19	C20	1.380(5)	C53	B2	1.618(4)
C20	C21	1.371(5)	C54	C55	1.368(4)
C21	C22	1.364(5)	C55	C56	1.372(5)
C22	C23	1.385(4)	C56	C57	1.363(5)
C24	C25	1.395(4)	C57	C58	1.378(4)
C24	C29	1.387(4)	C59	C60	1.536(10)

Atom	Atom	Length (Å)	Atom	Atom	Length (Å)
C24	B1	1.617(4)	C60	C61	1.522(11)
C25	C26	1.383(4)	C61	C62	1.530(7)
C26	C27	1.366(5)	C62	C63	1.524(11)
C27	C28	1.385(5)	C63	C64	1.509(9)
C28	C29	1.371(4)	C64	C65	1.503(11)
S3	C30	1.791(4)	C66	C67	1.501(10)
S3	C31	1.750(3)	C67	C68	1.530(9)
S4	C43	1.744(3)	C68	C69	1.520(9)
S4	C46	1.786(4)	C69	C70	1.507(8)
F11	C48	1.356(3)	C70	C71	1.541(8)
F12	C49	1.356(3)	C71	C72	1.511(10)

Table S17 | Bond angles for **(SMe-BPh$^{F}_{2}$)$_2$ · C$_7$H$_{16}$**.

Atom	Atom	Atom	Angle (˚)	Atom	Atom	Atom	Angle (˚)
C2	S1	C1	104.45(17)	C36	C31	S3	124.4(2)
C14	S2	C17	103.12(16)	C36	C31	C32	118.6(3)
C8	O1	B1	117.1(2)	C33	C32	C31	120.4(3)
C10	O2	B1	117.1(2)	C32	C33	C34	121.2(3)
C3	C2	S1	125.6(3)	C33	C34	C37	119.7(3)
C7	C2	S1	115.6(2)	C35	C34	C33	118.0(3)
C7	C2	C3	118.8(3)	C35	C34	C37	122.3(3)
C4	C3	C2	120.3(3)	C36	C35	C34	121.4(3)
C3	C4	C5	120.6(3)	C35	C36	C31	120.4(3)
C4	C5	C6	119.1(3)	O3	C37	C34	115.0(3)
C4	C5	C8	120.5(3)	O3	C37	C38	120.1(3)
C6	C5	C8	120.3(3)	C38	C37	C34	124.8(3)
C7	C6	C5	120.2(3)	C37	C38	C39	119.6(3)
C6	C7	C2	121.0(3)	O4	C39	C38	119.8(3)
O1	C8	C5	115.7(3)	O4	C39	C40	114.8(3)
O1	C8	C9	120.0(3)	C38	C39	C40	125.5(3)
C9	C8	C5	124.4(3)	C41	C40	C39	119.8(3)
C10	C9	C8	119.5(3)	C41	C40	C45	119.1(3)
O2	C10	C9	119.8(3)	C45	C40	C39	121.1(3)
O2	C10	C11	116.1(3)	C40	C41	C42	121.0(3)
C9	C10	C11	124.2(3)	C41	C42	C43	120.4(3)
C12	C11	C10	120.3(3)	C42	C43	S4	125.4(3)
C16	C11	C10	121.4(3)	C44	C43	S4	115.9(2)
C16	C11	C12	118.3(3)	C44	C43	C42	118.7(3)
C13	C12	C11	120.6(3)	C45	C44	C43	120.7(3)
C12	C13	C14	121.4(3)	C44	C45	C40	120.1(3)
C13	C14	S2	118.2(2)	C48	C47	C52	113.4(3)
C13	C14	C15	118.0(3)	C48	C47	B2	126.6(3)
C15	C14	S2	123.8(2)	C52	C47	B2	119.8(3)
C16	C15	C14	120.8(3)	F11	C48	C47	120.5(3)
C15	C16	C11	121.0(3)	F11	C48	C49	115.6(3)
C19	C18	B1	119.1(3)	C49	C48	C47	123.9(3)
C23	C18	C19	113.8(3)	F12	C49	C48	120.6(3)
C23	C18	B1	127.1(3)	F12	C49	C50	119.8(3)
F1	C19	C18	119.5(3)	C50	C49	C48	119.6(3)
F1	C19	C20	116.1(3)	F13	C50	C49	120.4(3)
C20	C19	C18	124.4(3)	F13	C50	C51	120.5(3)
F2	C20	C19	120.9(3)	C49	C50	C51	119.1(3)
F2	C20	C21	120.6(3)	F14	C51	C50	119.8(3)
C21	C20	C19	118.6(3)	F14	C51	C52	120.8(3)
F3	C21	C20	119.6(3)	C52	C51	C50	119.4(3)
F3	C21	C22	120.2(3)	F15	C52	C47	119.1(3)
C22	C21	C20	120.2(3)	F15	C52	C51	116.5(3)

Atom	Atom	Atom	Angle (°)	Atom	Atom	Atom	Angle (°)
F4	C22	C21	120.5(3)	C51	C52	C47	124.4(3)
F4	C22	C23	120.3(3)	C54	C53	C58	114.0(3)
C21	C22	C23	119.2(3)	C54	C53	B2	119.6(3)
F5	C23	C18	120.3(3)	C58	C53	B2	126.4(3)
F5	C23	C22	115.9(3)	F16	C54	C53	119.1(3)
C22	C23	C18	123.8(3)	F16	C54	C55	116.4(3)
C25	C24	B1	126.7(3)	C55	C54	C53	124.5(3)
C29	C24	C25	114.3(3)	F17	C55	C54	121.1(3)
C29	C24	B1	119.0(3)	F17	C55	C56	120.0(3)
F6	C25	C24	121.0(3)	C54	C55	C56	118.9(3)
F6	C25	C26	115.9(3)	F18	C56	C55	120.3(3)
C26	C25	C24	123.1(3)	F18	C56	C57	120.1(3)
F7	C26	C25	120.9(3)	C57	C56	C55	119.6(3)
F7	C26	C27	119.4(3)	F19	C57	C56	119.5(3)
C27	C26	C25	119.7(3)	F19	C57	C58	120.6(3)
F8	C27	C26	120.1(3)	C56	C57	C58	119.8(3)
F8	C27	C28	120.3(3)	F20	C58	C53	121.1(3)
C26	C27	C28	119.7(3)	F20	C58	C57	115.8(3)
F9	C28	C27	119.9(3)	C57	C58	C53	123.1(3)
F9	C28	C29	121.3(3)	O3	B2	C47	110.6(2)
C29	C28	C27	118.8(3)	O3	B2	C53	108.7(2)
F10	C29	C24	118.8(3)	O4	B2	O3	107.5(2)
F10	C29	C28	116.8(3)	O4	B2	C47	108.7(2)
C28	C29	C24	124.4(3)	O4	B2	C53	110.5(2)
O1	B1	O2	107.5(2)	C53	B2	C47	110.8(2)
O1	B1	C18	107.8(2)	C61	C60	C59	114.3(11)
O1	B1	C24	110.5(2)	C60	C61	C62	114.4(9)
O2	B1	C18	111.3(2)	C63	C62	C61	112.1(8)
O2	B1	C24	108.0(2)	C64	C63	C62	118.3(10)
C24	B1	C18	111.7(2)	C65	C64	C63	117.1(11)
C31	S3	C30	103.31(17)	C66	C67	C68	113.7(10)
C43	S4	C46	103.90(16)	C69	C68	C67	111.5(7)
C37	O3	B2	116.8(2)	C70	C69	C68	115.2(6)
C39	O4	B2	117.6(2)	C69	C70	C71	113.6(7)
C32	C31	S3	117.0(3)	C72	C71	C70	113.7(8)

Table S18 | Torsion angles for **(SMe-BPh$^{F}_{2}$)$_2$ · C$_7$H$_{16}$**.

Atom	Atom	Atom	Atom	Angle (˚)	Atom	Atom	Atom	Atom	Angle (˚)
S1	C2	C3	C4	178.7(2)	F11	C48	C49	C50	-179.4(3)
S1	C2	C7	C6	-178.7(2)	F12	C49	C50	F13	-0.7(5)
S2	C14	C15	C16	-179.5(2)	F12	C49	C50	C51	180.0(3)
F1	C19	C20	F2	-0.2(5)	F13	C50	C51	F14	0.6(5)
F1	C19	C20	C21	-179.4(3)	F13	C50	C51	C52	-179.0(3)
F2	C20	C21	F3	-0.5(5)	F14	C51	C52	F15	-0.1(4)
F2	C20	C21	C22	-179.7(3)	F14	C51	C52	C47	-180.0(3)
F3	C21	C22	F4	0.6(4)	F16	C54	C55	F17	0.1(5)
F3	C21	C22	C23	-178.8(3)	F16	C54	C55	C56	178.9(4)
F4	C22	C23	F5	-0.1(4)	F17	C55	C56	F18	-0.5(7)
F4	C22	C23	C18	180.0(3)	F17	C55	C56	C57	-178.8(4)
F6	C25	C26	F7	1.1(5)	F18	C56	C57	F19	0.8(7)
F6	C25	C26	C27	-178.2(3)	F18	C56	C57	C58	179.7(4)
F7	C26	C27	F8	-1.0(5)	F19	C57	C58	F20	-0.2(6)
F7	C26	C27	C28	178.5(3)	F19	C57	C58	C53	-179.9(4)
F8	C27	C28	F9	-1.1(5)	O3	C37	C38	C39	-11.5(4)
F8	C27	C28	C29	-179.7(3)	O4	C39	C40	C41	9.7(4)
F9	C28	C29	F10	2.0(5)	O4	C39	C40	C45	-173.0(3)
F9	C28	C29	C24	-177.0(3)	C30	S3	C31	C32	-178.2(2)
O1	C8	C9	C10	-12.6(4)	C30	S3	C31	C36	1.6(3)
O2	C10	C11	C12	14.0(4)	C31	C32	C33	C34	0.3(5)
O2	C10	C11	C16	-167.3(3)	C32	C31	C36	C35	0.1(4)
C1	S1	C2	C3	0.4(3)	C32	C33	C34	C35	0.3(4)
C1	S1	C2	C7	-179.3(3)	C32	C33	C34	C37	-178.3(3)
C2	C3	C4	C5	-0.1(5)	C33	C34	C35	C36	-0.7(4)
C3	C2	C7	C6	1.6(5)	C33	C34	C37	O3	-11.5(4)
C3	C4	C5	C6	2.0(4)	C33	C34	C37	C38	169.8(3)
C3	C4	C5	C8	-174.8(3)	C34	C35	C36	C31	0.5(4)
C4	C5	C6	C7	-2.1(4)	C34	C37	C38	C39	167.2(3)
C4	C5	C8	O1	-10.7(4)	C35	C34	C37	O3	170.0(3)
C4	C5	C8	C9	169.5(3)	C35	C34	C37	C38	-8.7(5)
C5	C6	C7	C2	0.3(5)	C36	C31	C32	C33	-0.5(5)
C5	C8	C9	C10	167.3(3)	C37	O3	B2	O4	44.8(3)
C6	C5	C8	O1	172.6(3)	C37	O3	B2	C47	-73.7(3)
C6	C5	C8	C9	-7.2(5)	C37	O3	B2	C53	164.4(2)
C7	C2	C3	C4	-1.6(5)	C37	C34	C35	C36	177.8(3)
C8	O1	B1	O2	45.4(3)	C37	C38	C39	O4	11.9(4)
C8	O1	B1	C18	-74.6(3)	C37	C38	C39	C40	-167.3(3)
C8	O1	B1	C24	163.0(2)	C38	C39	C40	C41	-171.0(3)
C8	C5	C6	C7	174.7(3)	C38	C39	C40	C45	6.3(5)
C8	C9	C10	O2	13.0(4)	C39	O4	B2	O3	-44.7(3)
C8	C9	C10	C11	-165.7(3)	C39	O4	B2	C47	75.1(3)
C9	C10	C11	C12	-167.3(3)	C39	O4	B2	C53	-163.2(2)

Atom	Atom	Atom	Atom	Angle (˚)	Atom	Atom	Atom	Atom	Angle (˚)
C9	C10	C11	C16	11.5(4)	C39	C40	C41	C42	176.5(3)
C10	O2	B1	O1	-44.9(3)	C39	C40	C45	C44	-175.7(3)
C10	O2	B1	C18	72.9(3)	C40	C41	C42	C43	-0.6(5)
C10	O2	B1	C24	-164.2(2)	C41	C40	C45	C44	1.6(4)
C10	C11	C12	C13	179.1(3)	C41	C42	C43	S4	-179.2(2)
C10	C11	C16	C15	-178.6(3)	C41	C42	C43	C44	1.3(5)
C11	C12	C13	C14	-0.4(5)	C42	C43	C44	C45	-0.6(5)
C12	C11	C16	C15	0.2(4)	C43	C44	C45	C40	-0.9(5)
C12	C13	C14	S2	179.9(2)	C45	C40	C41	C42	-0.9(4)
C12	C13	C14	C15	0.2(4)	C46	S4	C43	C42	5.9(3)
C13	C14	C15	C16	0.3(4)	C46	S4	C43	C44	-174.7(3)
C14	C15	C16	C11	-0.5(4)	C47	C48	C49	F12	-179.7(3)
C16	C11	C12	C13	0.2(4)	C47	C48	C49	C50	1.1(5)
C17	S2	C14	C13	179.3(2)	C48	C47	C52	F15	-179.3(2)
C17	S2	C14	C15	-1.0(3)	C48	C47	C52	C51	0.6(4)
C18	C19	C20	F2	180.0(3)	C48	C47	B2	O3	-19.1(4)
C18	C19	C20	C21	0.8(5)	C48	C47	B2	O4	-137.0(3)
C19	C18	C23	F5	-179.1(3)	C48	C47	B2	C53	101.5(3)
C19	C18	C23	C22	0.9(4)	C48	C49	C50	F13	178.6(3)
C19	C18	B1	O1	-51.6(3)	C48	C49	C50	C51	-0.7(5)
C19	C18	B1	O2	-169.1(3)	C49	C50	C51	F14	180.0(3)
C19	C18	B1	C24	70.1(4)	C49	C50	C51	C52	0.4(5)
C19	C20	C21	F3	178.7(3)	C50	C51	C52	F15	179.5(3)
C19	C20	C21	C22	-0.5(5)	C50	C51	C52	C47	-0.4(5)
C20	C21	C22	F4	179.8(3)	C52	C47	C48	F11	179.5(2)
C20	C21	C22	C23	0.4(5)	C52	C47	C48	C49	-1.0(4)
C21	C22	C23	F5	179.3(3)	C52	C47	B2	O3	165.8(3)
C21	C22	C23	C18	-0.6(5)	C52	C47	B2	O4	48.0(4)
C23	C18	C19	F1	179.2(3)	C52	C47	B2	C53	-73.6(3)
C23	C18	C19	C20	-1.0(5)	C53	C54	C55	F17	179.1(3)
C23	C18	B1	O1	131.8(3)	C53	C54	C55	C56	-2.2(6)
C23	C18	B1	O2	14.2(4)	C54	C53	C58	F20	179.6(3)
C23	C18	B1	C24	-106.6(3)	C54	C53	C58	C57	-0.8(5)
C24	C25	C26	F7	-179.3(3)	C54	C53	B2	O3	54.9(4)
C24	C25	C26	C27	1.4(5)	C54	C53	B2	O4	172.7(3)
C25	C24	C29	F10	178.8(3)	C54	C53	B2	C47	-66.8(4)
C25	C24	C29	C28	-2.2(5)	C54	C55	C56	F18	-179.3(4)
C25	C24	B1	O1	9.4(4)	C54	C55	C56	C57	2.5(7)
C25	C24	B1	O2	126.8(3)	C55	C56	C57	F19	179.1(4)
C25	C24	B1	C18	-110.6(3)	C55	C56	C57	C58	-2.0(7)
C25	C26	C27	F8	178.3(3)	C56	C57	C58	F20	-179.1(4)
C25	C26	C27	C28	-2.2(6)	C56	C57	C58	C53	1.2(7)
C26	C27	C28	F9	179.3(3)	C58	C53	C54	F16	-179.8(3)
C26	C27	C28	C29	0.8(5)	C58	C53	C54	C55	1.3(5)

Atom	Atom	Atom	Atom	Angle (˚)	Atom	Atom	Atom	Atom	Angle (˚)
C27	C28	C29	F10	-179.5(3)	C58	C53	B2	O3	-127.4(3)
C27	C28	C29	C24	1.5(5)	C58	C53	B2	O4	-9.7(4)
C29	C24	C25	F6	-179.7(3)	C58	C53	B2	C47	110.8(3)
C29	C24	C25	C26	0.8(5)	B2	O3	C37	C34	162.2(2)
C29	C24	B1	O1	-171.7(3)	B2	O3	C37	C38	-19.0(4)
C29	C24	B1	O2	-54.4(4)	B2	O4	C39	C38	18.5(4)
C29	C24	B1	C18	68.3(4)	B2	O4	C39	C40	-162.2(2)
B1	O1	C8	C5	161.3(2)	B2	C47	C48	F11	4.2(4)
B1	O1	C8	C9	-18.9(4)	B2	C47	C48	C49	-176.3(3)
B1	O2	C10	C9	17.9(4)	B2	C47	C52	F15	-3.6(4)
B1	O2	C10	C11	-163.2(2)	B2	C47	C52	C51	176.3(3)
B1	C18	C19	F1	2.1(4)	B2	C53	C54	F16	-1.8(4)
B1	C18	C19	C20	-178.0(3)	B2	C53	C54	C55	179.2(3)
B1	C18	C23	F5	-2.3(5)	B2	C53	C58	F20	1.8(5)
B1	C18	C23	C22	177.6(3)	B2	C53	C58	C57	-178.6(4)
B1	C24	C25	F6	-0.8(5)	C59	C60	C61	C62	-175.8(14)
B1	C24	C25	C26	179.7(3)	C60	C61	C62	C63	160(3)
B1	C24	C29	F10	-0.2(4)	C61	C62	C63	C64	-180.0(14)
B1	C24	C29	C28	178.7(3)	C62	C63	C64	C65	-56(3)
S3	C31	C32	C33	179.3(2)	C66	C67	C68	C69	-177.7(12)
S3	C31	C36	C35	-179.7(2)	C67	C68	C69	C70	-178.0(6)
S4	C43	C44	C45	179.9(2)	C68	C69	C70	C71	-172.8(8)
F11	C48	C49	F12	-0.1(4)	C69	C70	C71	C72	171.0(9)

References

1. O. V. Dolomanov, L. J. Bourhis, R. J. Gildea, J. A. K. Howard and H. Puschmann, *J. Appl. Crystallogr.*, 2009, **42**, 339-341.
2. G. M. Sheldrick, *Acta Crystallogr., Sect. A: Found. Adv.*, 2015, **71**, 3-8.
3. G. M. Sheldrick, *Acta Crystallogr., Sect. C: Struct. Chem.*, 2015, **71**, 3-8.
4. I. J. Bruno, J. C. Cole, P. R. Edgington, M. Kessler, C. F. Macrae, P. McCabe, J. Pearson and R. Taylor, *Acta Crystallogr., Sect. B: Struct. Sci.*, 2002, **58**, 389-397.
5. C. F. Macrae, P. R. Edgington, P. McCabe, E. Pidcock, G. P. Shields, R. Taylor, M. Towler and J. van De Streek, *J. Appl. Crystallogr.*, 2006, **39**, 453-457.
6. A. L. Spek, *J. Appl. Crystallogr.*, 2003, **36**, 7-13.
7. L. Venkataraman, J. E. Klare, I. W. Tam, C. Nuckolls, M. S. Hybertsen and M. L. Steigerwald, *Nano Lett.*, 2006, **6**, 458-462.
8. L. Venkataraman, J. E. Klare, C. Nuckolls, M. S. Hybertsen and M. L. Steigerwald, *Nature*, 2006, **442**, 904-907.
9. B. Xu and N. J. Tao, *Science*, 2003, **301**, 1221-1223.
10. B. J. van Wees, H. van Houten, C. W. Beenakker, J. G. Williamson, L. P. Kouwenhoven, D. van der Marel and C. T. Foxon, *Phys. Rev. Lett.*, 1988, **60**, 848-850.
11. S. G. Balasubramani, G. P. Chen, S. Coriani, M. Diedenhofen, M. S. Frank, Y. J. Franzke, F. Furche, R. Grotjahn, M. E. Harding, C. Hättig, A. Hellweg, B. Helmich-Paris, C. Holzer, U. Huniar, M. Kaupp, A. Marefat Khah, S. Karbalaei Khani, T. Muller, F. Mack, B. D. Nguyen, S. M. Parker, E. Perlt, D. Rappoport, K. Reiter, S. Roy, M. Rückert, G. Schmitz, M. Sierka, E. Tapavicza, D. P. Tew, C. van Wüllen, V. K. Voora, F. Weigend, A. Wodyński and J. M. Yu, *J. Chem. Phys.*, 2020, **152**, 184107.
12. A. D. Becke, *Phys. Rev. A*, 1988, **38**, 3098-3100.
13. J. P. Perdew, *Phys. Rev. B*, 1986, **33**, 8822-8824.
14. F. Weigend and R. Ahlrichs, *Phys. Chem. Chem. Phys.*, 2005, **7**, 3297-3305.
15. F. Pauly, J. K. Viljas, U. Huniar, M. Häfner, S. Wohlthat, M. Bürkle, J. C. Cuevas and G. Schön, *New J. Phys.*, 2008, **10**, 125019.
16. M. Bürkle, J. K. Viljas, T. J. Hellmuth, E. Scheer, F. Weigend, G. Schön and F. Pauly, *Phys. Status Solidi B*, 2013, **250**, 2468-2480.
17. J. C. Cuevas and E. Scheer, *Molecular Electronics: An Introduction to Theory and Experiment*, World Scientific, 2nd edn., 2017.
18. T. Markussen, C. J. Jin and K. S. Thygesen, *Phys. Status Solidi B*, 2013, **250**, 2394-2402.
19. D. J. Mowbray, G. Jones and K. S. Thygesen, *J. Chem. Phys.*, 2008, **128**, 111103.
20. S. Y. Quek, L. Venkataraman, H. J. Choi, S. G. Louie, M. S. Hybertsen and J. B. Neaton, *Nano Lett.*, 2007, **7**, 3477-3482.
21. L. A. Zotti, M. Bürkle, F. Pauly, W. Lee, K. Kim, W. Jeong, Y. Asai, P. Reddy and J. C. Cuevas, *New J. Phys.*, 2014, **16**, 015004.
22. W. M. Schosser, C. Hsu, P. Zwick, K. Beltako, D. Dulić, M. Mayor, H. S. J. van der Zant and F. Pauly, *Nanoscale*, 2022, **14**, 984-992.
23. K. Yoshizawa, T. Tada and A. Staykov, *J. Am. Chem. Soc.*, 2008, **130**, 9406-9413.
24. P. von Ragué Schleyer, C. Maerker, A. Dransfeld, H. Jiao and N. J. R. van Eikema Hommes, *J. Am. Chem. Soc.*, 1996, **118**, 6317-6318.
25. M. J. Frisch, G. W. Trucks, H. B. Schlegel, G. E. Scuseria, M. A. Robb, J. R. Cheeseman, G. Scalmani, V. Barone, G. A. Petersson, H. Nakatsuji, X. Li, M. Caricato, A. V. Marenich, J. Bloino, B. G. Janesko, R. Gomperts, B. Mennucci, H. P. Hratchian, J. V. Ortiz, A. F. Izmaylov, J. L. Sonnenberg, D. Williams-Young, F. Ding, F. Lipparini, F. Egidi, J. Goings, B. Peng, A. Petrone, T. Henderson, D. Ranasinghe, V. G. Zakrzewski, J. Gao, N. Rega, G. Zheng, W. Liang, M. Hada, M. Ehara, K. Toyota, R. Fukuda, J. Hasegawa, M. Ishida, T. Nakajima, Y. Honda, O. Kitao, H. Nakai, T. Vreven, K. Throssell, J. A. Montgomery Jr., J. E. Peralta, F. Ogliaro, M. J. Bearpark, J. J. Heyd, E. N. Brothers, K. N. Kudin, V. N. Staroverov, T. A. Keith, R. Kobayashi, J. Normand, K. Raghavachari, A. P. Rendell, J. C. Burant, S. S. Iyengar, J. Tomasi, M. Cossi, J. M. Millam, M. Klene, C. Adamo, R. Cammi, J. W. Ochterski, R. L. Martin, K. Morokuma, O. Farkas, J. B. Foresman and D. J. Fox, Gaussian 16, Rev. B.01, Wallingford CT, 2016.